UNIVERSITY OF CALIFORNIA
SANTA CRUZ

Development of CRISPR/Cas9 *in vivo* bladder cancer models

A thesis submitted in partial satisfaction of the
requirements for the degree of

MASTER OF SCIENCE

in

MOLECULAR, CELLULAR, DEVELOPMENTAL BIOLOGY

by

Ofir Stefanson

December 2019

The Thesis of Ofir Stefanson
is approved:

_____

Professor Zhu Wang

_____

Professor Bin Chen

_____

Professor David Feldheim

_____

Quentin Williams

Vice Provost and Dean of Graduate Studies

Table of Contents

List of Figures **v**

List of tables **vi**

Abstract **vii**

Dedication **ix**

Acknowledgements **x**

Chapter 1: Introduction **1**

1.1 Bladder cancer prevalence 1

1.2 Bladder Biology 1

1.3 Bladder Cancer Biology 4

1.4 Molecular landscape of bladder cancer 6

1.5 Bladder cancer modeling *in vivo* 9

1.6 CRISPR/Cas9 and cancer modeling 11

1.7 Project objective 12

Chapter 2: Methods **14**

2.1 Mouse strain and procedures 14

2.2 Plasmid construction 14

2.3 sgRNA validation 15

2.4 sgPTEN-TP53 plasmid validation 16

2.5 Electroporation 16

2.6 Tissue collection and processing 17

2.7 Histology 17

2.8 Immunofluorescence staining 18

2.9 Imaging 19

2.10 Cell dissociation, and deep sequencing 19

Chapter 3: Results **21**

3.1 Development and testing of plasmid delivery by electroporation 21

3.2 Design and validation TP53 and PTEN sgRNA plasmid 24

3.3 *In vivo* validation of sgPTEN-TP53 26

3.4 CRISPR/Cas9 mutation induces tumors in the bladder 28
3.5 Pathology of CRISPR/Cas9 induced bladder tumors 32
Chapter 4: Discussion **37**
Appendix **40**
References **41**

List of Figures

Figure 1.1: Cell types of mouse urothelium. 4

Figure 1.2: Urothelial carcinoma stage classification. 6

Figure 3.1: Bladder urothelium electroporation technique. 22

Figure 3.2: Electroporation successfully delivers plasmids into mouse bladder urothelium 23

Figure 3.3: Co-electroporation of plasmids into the bladder urothelium. 24

Figure 3.4: Validation of sgPTEN and sgTP53 *in vitro*. 25

Figure 3.5: Validation of sgPTEN-TP53 plasmid *in vitro.* 26

Figure 3.6: *In vivo* sgPTEN-TP53 mutation analysis. 27

Figure 3.7: Validation of Cas9 expression and sgPTEN-TP53 electroporation in the urothelium. 29

Figure 3.8: Histology of control Cas9 bladders. 30

Figure 3.9: Histology of bladders electroporated with of sgRNAs targeting TP53 and PTEN. 31-33

Figure 3.10: Pathology of control Cas9 bladders. 34

Figure 3.11: Increased cell proliferation and basal cell layer due to sgPTEN-TP53 in tumor resembling carcinoma. 35

Figure 3.12: sgPTEN-TP53 induced an increase in the CK5 basal cell layer. 36

List of Tables

Table 2.1: Primary antibodies used for immunofluorescence staining 19

Abstract

Development of CRISPR/Cas9 *in vivo* bladder cancer models

by

Ofir Stefanson

Bladder cancer prevalence is high, and patients diagnosed with this malignancy incur a high economic burden and a poor-quality lifestyle. The majority of bladder cancers are urothelial carcinomas, with two subtypes: papillary non-invasive and muscle-invasive bladder cancer. The muscle-invasive subtype is associated with a poor prognosis and a high mutation frequency. Nevertheless, there are no efficient in vivo bladder cancer models in the field to study disease initiation and progression. Thus far, most in vivo bladder cancer models rely on the Cre-LoxP system. However, this technique is expensive and time-consuming. Furthermore, it depends on available mice with floxed alleles for target genes. Recently, CRISPR/Cas9 has been used to study cancer and overcomes the hurdles of Cre-LoxP models. The objective of this work is to determine if CRISPR/Cas9 can be coopted for bladder cancer research in vivo. As-proof-of concept CRISPR/Cas9 was used to recapitulate a Cre-LoxP muscle-invasive bladder mouse model produced by knockout of tumor suppressors PTEN and TP53. Single guide RNAs targeting TP53 and PTEN were delivered into the bladder urothelium of Cas9 expressing mice by a novel electroporation approach. Histological and pathological characterization of bladders indicated tumor

development in 2 mice, with a tumor penetrance of 33%. Tumors phenotypically resembled hyperplasia and papillary carcinoma, with an increase of CK5 positive basal layer. Papillary tumors exhibited an increase in cell proliferation compared to controls. Overall, optimizations are required in order to use the CRISPR/Cas9 technique for in vivo bladder cancer models.

Dedication

To Saba

שבתי לוי

I miss you and think about you every day.

Acknowledgements

I want to acknowledge my PI and mentor, Zhu Wang. Thank you for letting me in the lab to work on this project, and for your leadership, support, and intellectual input throughout my time in the lab. Zhu is one of the most intelligent and hardworking people I ever met and something that I strive to be.

To Chuan Yu, a postdoc in the lab. His guidance and creativity are what made this project possible. Chuan started this project, and I worked with him throughout the duration of this project. This project would not have been possible without him. Good luck with the next steps.

To Yueli Liu, aka Lily. Thank you so much for training me in every lab technique that I used.

To Cory Horten, Lily, and Chuan. Thank you for being great lab mates and friends during the last few years.

Chapter 1: Introduction

1.1 Bladder cancer prevalence

Urinary bladder cancer (BCa) is the 4th most common cancer in men and the 15th most common cancer in women. In 2019, there were 80,470 new diageneses and 17,670 death caused by bladder cancer in the United States alone. Bladder cancer incidence increases in geriatrics. 9 of 10 cases occur in people over the age of 55, and are three times more frequent in men than women (Siegel et al., 2019). The most common risk factor for BCa is carcinogen exposure due to cigarette smoking. BCa Patients typically incurred a lifelong economic burden due to its high recurrence rate and the need for surveillance throughout the patient's lifetime, and high cost of treatment (Yeung et al., 2014) (Sanli et al., 2017).

1.2 Bladder Biology

The bladder is a hollow organ and its primary function is urine storage and to maintain the physiological composition of urine developed in the kidneys. The bladder is composed of a stratified epithelium layer, termed the urothelium, surrounds by the bladder lumen. The urothelium is encapsulated by the lamina propria, detrusor muscle, and perivesical fat layer. The urothelium is subdivided

into a single layer of umbrella cells, several intermediate cell layers, and a single basal cell layer (Fig 1.1) (Hicks, 1975) (Jost et al., 1989).

The umbrella cells are highly differentiated, and function to accommodate changes in volume and the high impermeability of the bladder, through a specialized apical membrane, and tight junctions between neighboring umbrella cells. The apical membrane is composed of plaque regions surrounded by hinge regions. The plaque region makes up about 90% of the membrane and are composed of umbrella cell-specific transmembrane proteins, Uroplakin (UP Ia, Ib, II, IIIa, and IIIb), which arrange as a hexagonal ring, termed the asymmetric membrane units. These units form an asymmetric membrane within the plaque, causing the lumen facing membrane to be twice as thick as the cytoplasmic membrane (Khandelwal et al., 2009). Physiologically these plaques are essential for the permeability of the urothelium, as ablation of UPII or IIIa resulted in increased permeability (Kong et al., 2004)(Hu et al., 2000). Umbrella cells contain a high density of cytoplasmic vesicles (termed discoidal/fusiform-shaped vesicles or DFV) that incorporate into the apical membrane by endocytosis and exostosis as a response to changing bladder volumes. The DFVs deliver UPs to the apical membrane (Khandelwal et al., 2009) (Wu et al., 2009). Umbrella cells express high levels of cytokeratin (CK) 18 and 20 (Kobayashi et al., 2015).

Intermediate cells form several layers beneath the umbrella cells. The number of layers is species dependent. In humans the intermediate cells make up 5 layers, while one to two layers are observed in rodents (Jost et al., 1989)

(Khandelwal et al., 2009). Intermediate cells are partially differentiated and undergo differentiation into umbrella cells in response to loss or damage (Lavelle et al., 2002) (Veranič et al., 2009). Basal cells are thought to be progenitors of the urothelium and can regenerate all urothelial cell types (Shin et al., 2011) (Papafotiou et al., 2016). However, there is disagreement in the field, as some suggest that the urothelial cell types arise from different progenitors (Colopy et al., 2014) (Sun et al., 2014). Basal cells express high levels of CK5, CK14, p63. Intermediate cells express the same markers but at lower levels compared to basal cells (Kobayashi et al., 2015).

The adult urothelium is quiescent and undergoes a slow turnover rate (Stewart et al., 1980) (Jost and Potten, 1986). The mouse bladder serves as a good model for bladder cancer since it is morphologically similar to the human bladder, although it rarely develops cancer naturally (Clayson et al., 1995).

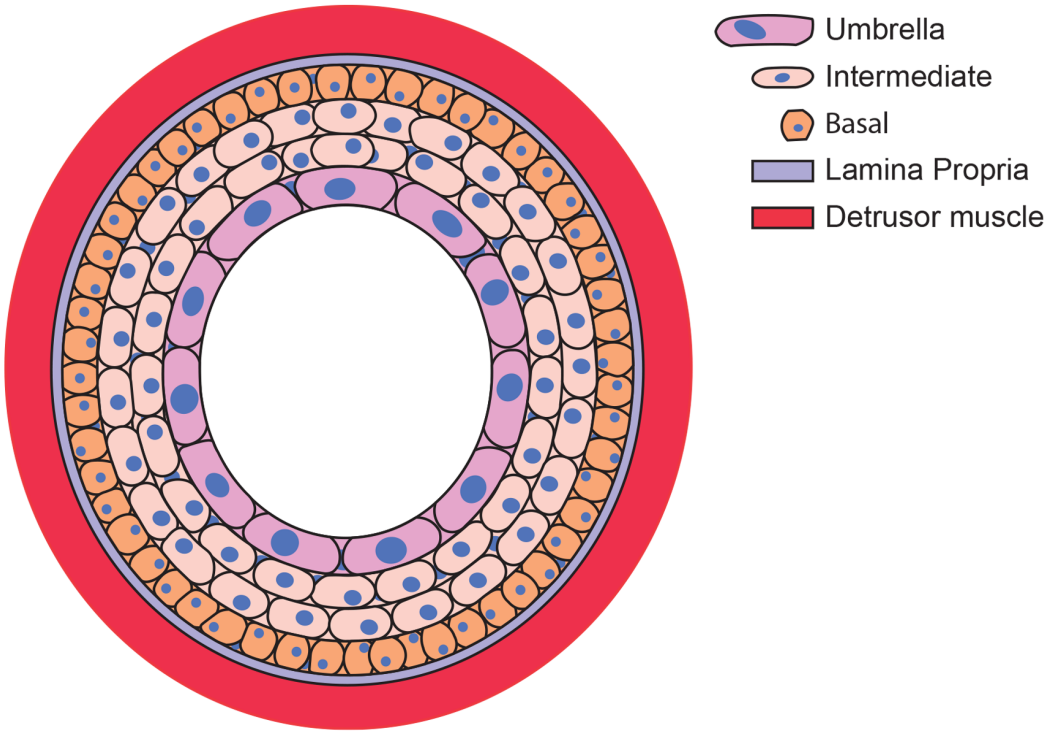

Figure 1.1: Cell types of mouse urothelium.
The mouse bladder lumen is enclosed by a stratified epithelium, the urothelium, consisting of the apical facing umbrella cells (UPs and CK18 positive), one to two layers of intermediate (low levels of CK5, CK18 and UPs) cells, and basal cells (CK5 positive). The lamina propria and the detrusor muscle encapsulate the urothelium.

1.3 Bladder Cancer Biology

Urothelial carcinoma is the most common form of BCa, with two main histopathological subtypes, papillary non-muscle invasive BCa (NMIBC) and solid muscle-invasive BCa (MIBC). Non-urothelial neoplasms are rare, only accounting for about 5% of bladder cancer cases (Dahm and Gschwend, 2003). NMIBC accounts for about 75% of bladder cancer diagnoses (Kamat et al., 2016).

NMIBC low-grade papillary tumors confined by the lamina propria (Ta), and high-grade papillary tumors invading the lamina propria (T1) (Fig 1.2). *Carcinoma in situ* (Tis) is a non-muscle invasive tumor considered to be a precursor of MIBC (Spruck et al., 1994). Surgical resections and immunotherapy or chemotherapy treatments are used for NMIBC, and patients generally exhibit a favorable prognosis. NMIBC tumors are likely to recur, and a small fraction progresses to muscle-invasive disease (Sanli et al., 2017).

The muscle-invasive subtype is described as non-papillary solid tumors and categorized by tumor invasion of the detrusor muscle (T2). Tumor progression to perivesical fat invasion is categorized as T3. MIBC tumors can potentially metastasize to the prostate, uterus, vagina, bowel (T4a), or the abdominal wall (T4b) (Fig 1.2). Patients diagnosed with MIBC have a poor prognosis, with a 5-year survival rate of about 50%. However, for metastatic cancer, the survival rate is about 15% (Kamat et al., 2016).

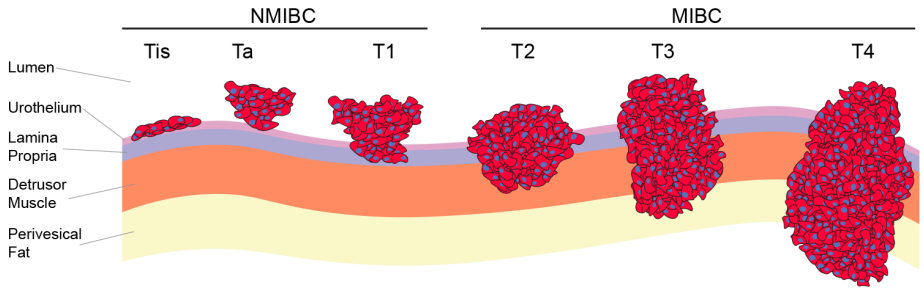

Figure 1.2: Urothelial carcinoma stage classification.
Bladder cancer (BCa) is classified as Non-muscle invasive BCa (NMIBC) and muscle-invasive BCa (MIBC). NMIBC tumors consists of papillary tumors, which are confined (Ta) or invade (T1) the lamina propria, and include *carcinoma in situ* (Tis). MIBC tumors invade the detrusor muscle (T2), the perivesical fat (T3), or metastasize to other tissue (T4). Stages classified using the Tumor, Node, metastasis system.

1.4 Molecular landscape of bladder cancer

Papillary NMIBC and solid MIBC arise from molecularly distinct pathogenic mechanisms. Loss of heterozygosity in chromosome 9 is an early event in bladder carcinogenesis common to both pathological subtypes. This deletion occurs in 50% of BCa cases and implicates tumor suppressors *TSC1* (9q34) and *CDKN2A* (9p21). *TSC1* is a negative regulator of mammalian target of rapamycin (mTOR) signaling pathway. The *CDKN2A* locus codes for p14arf and p16, which function as negative regulators of the cell cycle pathway (Lindgren et al., 2006)(van Oers et al., 2006).

Papillary tumors are typically genetically stable with diploid karyotypes (Hurst et al., 2012). A hallmark of low-grade papillary NMIBC tumors is the activating mutation in the gene *FGFR3*, with some studies reporting a mutation

frequency of about 60% (Tomlinson et al., 2007) (Pietzak et al., 2017). In cell culture, activation of FGFR3 leads to activation of the RAS-MAPK pathway, leading to increased cell proliferation and survival (di Martino et al., 2009). *PIK3CA* frequently incurs activating mutation in NMIBC, implicating the PI3K pathway (Pietzak et al., 2017). *PIK3CA* mutations commonly associate with *FGFR3* mutations (López-Knowles et al., 2006) (Platt et al., 2009) (Pietzak et al., 2017). Mutations to *STAG2*, a member of the cohesion complex, are associated with low-grade NMIBCA (Taylor et al., 2014) (Solomon et al., 2013) (Pietzak et al., 2017).

MIBC is characterized by genomic instability and a high frequency of mutations, averaging about 300 mutations per tumor sample. The most common genetic alterations in MIBC patients are mutations to the cell-cycle regulation pathway, altered in about 90% of MIBC cases. Frequently altered genes in the cell cycle pathway are: *TP53* (48% of cases), *RB1* (17%), and the *CDKN2A* locus (22%). (Robertson et al., 2017). *TP53* mutations are found in *carcinoma in situ* lesions and considered to be a precursor to MIBC development (Spruck et al., 1994) (Hartmann et al., 2002)(Hopman et al., 2002). *FGFR3* mutations are also present in MIBC samples; however, at a lower frequency than NMIBC. FGFR3 mutations are associated with lower-stages of MIBC. Alteration to members of the PI3K are also observed in MIBC. *PIK3CA* frequently incurs activating mutations. *PTEN* a Negative regulator of the PI3K pathway is frequently mutated in MIBC (Robertson et al., 2017) (Platt et al., 2009).

Both MIBC and NMIBC have a high mutation rate in the promoter region of the *TERT* (telomerase reverse transcriptase) gene. Frequent mutations to chromatin remodeling genes *KMT2D*, *KDM6A*, *ARID1A*, and *KMT2C* are observed in both BCa subtypes (Allory et al., 2014) (Robertson et al., 2017) (Pietzak et al., 2017).

Major research efforts have focused on characterizing the molecular subtypes of MIBC to assess the phenotypic heterogeneity within the disease and to correlate clinical outcomes and possible treatments (Robertson et al., 2017)(Sjödahl et al., 2017)(Seiler et al., 2017)(Hedegaard et al., 2016)(Rebouissou et al., 2014) (Choi et al., 2014)(Iyer et al., 2013). Subtype classifications among the studies vary, but distinct molecular subtypes have been identified: basal/squamous and luminal. The luminal subtype is molecularly heterogeneous presents papillary histology, and expresses Urothelial differentiation markers (CK20, Foxa1, and UPs). The Basal/squamous subtype expresses basal markers (CK5, CK14, CD44), and contains high mutation rates in the gene *TP53*. Additionally, the Robertson and Sjödahl studies also reported a neuronal subtype. Basal/squamous and neuronal subtypes are associated with worse prognosis and survival rates, compared to the luminal subtypes. A recent consensus study on 16 publicly available MIBC datasets indicated 6 molecular subtypes: luminal papillary, luminal non-specified, luminal unstable, stroma, basal/squamous, and neuroendocrine (Kamoun et al., 2019).

Overall, sequencing studies have improved the understanding of BCa, but more research is required to relate molecular subtypes to potential clinical therapeutics and characterize how genetic mutations impact carcinogenesis in the bladder.

1.5 Bladder cancer modeling *in vivo*

Research on the effect of genetic mutations on BCa development and progression is hindered by the lack of available *in vivo* models. There are two main models used for *in vivo* BCa research: chemical carcinogen exposure and genetically engineered mice (GEM). The majority of carcinogen-induced BCa models utilize n-butyl-n-(4-hydroxybutyl)nitrosamine (BBN), a chemical found in tobacco. It is usually delivered in drinking water to the mice. The BBN model is advantageous since it recapitulates human BCa progression and its phenotypes, including MIBC and metastatic BCa. BBN treatment results in tumors that are molecularly similar to human basal/squamous subtype, and incur frequent mutations to *TP53* (Saito et al., 2018). The disadvantages to the BBN carcinogenesis model are that cancer development and progression are inconsistent, and heterogenous BCa phenotypes develop. Furthermore, it is challenging to control genetic alterations using BBN.

The effects of specific genetic mutations on tumorigenesis have been studied using GEM models. The most common models utilize the Cre recombinase-mediated knockout, in which Cre excises DNA sequences between

two loxP sites via recombination. This system is used to generate mice in which a cell-type-specific promoter drives Cre expression to knockout genes flanked by loxP sites (floxed genes).

UP2 driven Cre expression (UP2-Cre) is a common bladder specific promoter used in BCa research. This promoter primarily functions in umbrella cells. Models utilized UP2-Cre to study the effect of common tumor suppress and oncogenes on bladder carcinogenesis. Co-knockout *TP53* and *RB1* results in rare instances of papillary NMIBC, however treatment with a low concentration of BBN induces MIBC in by 10 weeks in 50% of mice. In comparison, single inactivation of either *TP53* or *RB1* is not tumorigenic (He et al., 2009). *TP53* deficiency, in combination with oncogenic *HRAS* expression results in MIBC (He et al., 2015). Activation of oncogenic form *FGFR3* alone is insufficient in inducing urothelial carcinogenesis (Ahmad et al., 2011). However, *FGFR3* activation with *PTEN* deficiency results in hyperplasia (Foth et al., 2014). Recently, the UP3a-CreERT2 driver was used to knockout *TP53* and *PTEN* resulting mostly resulted in papillary tumors, but with some insistences of muscle-invasion. (Saito et al., 2018).

Models using non-urothelium specific Cre drivers have been utilized in BCa models. Adenovirus delivery of Cre to knockout *TP53* and *PTEN* resulted in a MIBC phenotype (Puzio-Kuter et al., 2009) . Adenovirus inactivation of *TP53* and activation oncogenic of *KRAS* results in urothelial hyperplasia (Yang et al., 2017). Basal cell driver, CK5-CreERT2, was used to knockout *PTEN* and *TP53*.

However, mice died due to carcinogenesis in other epithelial tissues (Saito et al., 2018).

In summary, the Cre-LoxP system enabled the investigation of specific gene mutations on BCa tumorigenesis but is inefficient, as typically, knockout of multiple alleles is required to observe a phenotype. This presents a challenge since the mutation load is high in BCa and generating mice with floxed alleles for multiple genes is expensive, time-consuming, and depends on the availability of genes with floxed alleles.

1.6 CRISPR/Cas9 and cancer modeling

CRISPR (or clustered regularly interspaced short palindromic repeats) is a sequence-specific genome editing system that was discovered in prokaryotes but was co-opted for use in mammalian systems. This system requires two components, Cas9 (CRISPR associated protein 9) endonuclease and single-guide RNA (sgRNA), which directs Cas9 to the target site. The sgRNA is composed of 17-20 nucleotide sequence complementary to the target locus (crRNA), and an RNA binding scaffold for Cas9 (tracrRNA) containing a PAM sequence (NGG). Cas9 cleaves the target sequence 3 nucleotides past the PAM. The cell repairs DNA cleavage by nonhomologous end-joining (NHEJ) or homology-directed repair (HDR) mechanisms. NHEJ results in insertion or deletions (indels) to the cleaved target sequence, and HDR utilizes the recombination machinery to repair the cleaved sequence using a template. In cancer research, the NHEJ is used to

mutate tumor suppressor genes by designing sgRNA to target specific candidate genes of interest. HDR was used to introduce oncogenic mutations by providing a template DNA of an oncogenic version of a gene (Wang et al., 2016).

The CRISPR/Cas9 system has been utilized for in vivo cancer modeling. Liver tumors were induced by hydrodynamic tail injection of plasmids containing Cas9 and sgRNAs targeting TP53 and PTEN, recapitulating the Cre-LoxP TP53 and PTEN knockout model (Xue et al., 2014). GEMMs expressing Cas9 were developed and utilized to model lung cancer by Adeno-associated virus delivery of sgRNAs targeting TP53, LKB1, and Kras in combination with an oncogenic Kras template, demonstrating CRISPR mediated HDR can be utilized for cancer modeling (Platt et al., 2014). Medulloblastoma and glioblastoma were generated by in utero electroporation of sgRNA targeting PTCH1, or a combination of TP53, PTEN, and NF1, respectively (Zuckermann et al., 2015). Furthermore, the CRISPR/Cas9 system can be used for mutagenesis of large gene sets by delivery of multiple sgRNA, as demonstrated in the liver and pancreas (Weber et al., 2015) (Maresch et al., 2016).

1.7 Project objective

The mutational burden in BCa is high, especially in the MIBC phenotype. The effects of many of the top mutated genes on BCa initiation and progression have yet to be characterized. The commonly used Cre-LoxP system is disadvantageous for this BCa research as multiple mutations are required for

carcinogenesis. Consequently, this technique is expensive and time-consuming due to the extensive breeding process. Additionally, the Cre-LoxP technique depends on available floxed alleles. The CRISPR/Cas9 cancer modeling approach overcomes the limitation of the Cre-LoxP system.

The objective of this project is to develop a new approach for BCa mouse models using CRISPR/Cas9. Described here is a novel technique for the delivery of plasmid into the urothelium mice by electroporation. This technique was utilized to study the effect of mutating tumor suppressors TP53 and PTEN, as knockout using Cre-LoxP induced MIBC in mice. Mutations to TP53 and PTEN were produced by electroporation of a plasmid containing sgRNAs targeting set gene into the bladders of mice ubiquitously expressing Cas9. The effects of CRISPR/Cas9 mutations to TP53 and PTEN on the bladder were histologically and pathologically characterized at different time points to determine the utility of this technique.

Chapter 2: Methods

2.1 Mouse strain and procedures

Animal experiments were performed with approval from the UC Santa Cruz Institutional Animal Care and Use Committee. Homozygous *R26-Cas9* mice (termed Cas9) (JAX stock #026179) (Platt et al., 2014) and wildtype mice were maintained in C57BL/6N background. Genotyping was performed on tail extracted genomic DNA by PCR using primer sequences: 5'-CTGGCTTCTGAGGACCG-3' (wildtype forward), 5'-AGCCTGCCCAGAAGACTCC-3' (wildtype reverse), 5'-GCTAACCATGTTCATGCCTTC-3' (mutant forward), and 5'-CTCCGTCGTGGTCCTTATAGT-3' (mutant reverse).

2.2 Plasmid construction

The plasmid containing sgRNAs targeting *PTEN* and *TP53* in mCherry vector (sgPTEN-TP53) was constructed by GeneScript. Sequence containing mouse U6 promoter (Das et al., 1988), sgRNA targeting *PTEN* (5'-AGATCGTTAGCAGAAACAAA-3') (Xue et al., 2014), sgRNA scaffold, spacer sequence (5'-TTTTTTTAGCCGAACTGTTTCACACTCACGCGTCCAAGGTCGGGCAGGAA-3'), human U6 promoter (Kunkel et al., 1986), and sgRNA targeting *TP53* (5'- CCTCGAGCTCCCTCTGAGCC-3' described) (Xue et al.,

2014) (full insert sequence in Supplementary Information 1) was cloned into AseI restriction site in mCherry-C2 (Addgene # 54563).

2.3 sgRNA validation

sgRNAs targeting PTEN or TP53 were cloned pX330 vector (Addgene #42230) (termed sgPTEN and sgTP53, respectively) and validated *in vitro* in NIH/3T3 cells (ATCC CRL-1658). Cells were plated in DMEM supplemented with FBS (10%) at 20% confluency 16 hours prior to transfection. Cells were transfected with 1ug of sgPTEN or sgTP53 and 0.5ug CAG-GFP (Addgene # 16664) (Zhao, 2006) using Lipofectamine LTX with PLUS Reagent (ThermoFisher Scientific #A12621) according to manufactures instructions. 24 hours post-transfection media was changed to fresh DMEM (10% FBS). Cells were sorted for positive GFP signal using FACS 72 hours-post transfections. Genomic DNA was used to amplify sgRNA target site using: 5'-TGCGAGGATTATCCGTCTTC-3' (*PTEN* forward), 5'-AACGTGGGAGTAGACGGATG -3' (*PTEN* reverse), 5'-TCTGTCCTCCATGTTCCTGG-3' (*TP53* forward), 5'-TTTCTCTCAGGCAAGGGGAG-3' (*TP53* reverse).
PCR parameters: 95°C 3:00 minutes, 35 cycles of 95°C for 30 seconds, 62°C for seconds, and 72°C for 1 minute, with a final extension at 72°C for 5 minutes. PCR amplicons were purified by adding 1 volume of isopropanol and 1/10 volume of sodium acetate, subsequentially washed with 70% ethanol and air

dried. Surveyor Assay (IDT #706020) was conducted on PCR amplicons according to manufactures instructions and analyzed on a 1% agarose gel.

2.4 sgPTEN-TP53 plasmid validation

NIH/3T3 cells were transfected as described in Section 2.3 with 1ug of sgPTEN-TP53 and 0.5ug pX330. Cells were sorted for positive mCherry signal using FACS 72 hours-post transfections. Genomic DNA used to generated amplicons as described in section 2.3. Amplicons were sent to Sequtech for single primer extension sequencing using *PTEN* forward and *TP53* forward primers.

2.5 Electroporation

Bladder electroporation performed as described by a technique developed by the Wang lab (Yu et al., 2018). Female mice were anesthetized using isoflurane vaporizer (VetEqiup #901806) set for 3% for induction and 2% for maintenance. Bladders were catheterized using a 24G catheter (Fisher scientific # 1484121). Veterinary lubricant was applied to the catheter and the urethral orifice prior to catherization. The bladder was depleted of urine and rinsed with PBS (80ul) 3 times by injection through the catheter. Then bladders were injected with plasmid solution consisting of 20ul of 1ug/ul plasmid and 1ul of Trypan blue stain. Subsequently, the urethral orifice was tied, the mouse skin and abdomen were cut to expose the bladder. Electroporation was conducted by grabbing the bladder using a 7mm platinum tweezertorde with ECM830 Electroporation

Generator (BTX #450052) set to the following parameters: 33V, 50ms working time, and 950ms interval time. Following electroporation, the abdomen and skin were sutured and clipped. See Supplementary Figure 1 for visual representation of electroporation technique. Plasmids electroporated: CAG-GFP (Addgene # 16664) (Zhao, 2006), pQC membrane CFP IX plasmid (Addgene # 37336; hereafter termed CFP plasmid) , mCherry-C2 (used as empty vector control), or sgPTEN-TP53.

2.6 Tissue collection and processing

Bladders were dissected and fixed using 4% paraformaldehyde (PFA) or with 10% formalin. PFA treated bladders were fixed for 5 hours. Subsequently slides were treated in 30% sucrose for 48 hours, and in 1:1 sucrose: OCT compound (Sakura) for 6 hours. Tissue were cryo-embedded in OCT at -80°C.

Formalin fixed bladders were fixed overnight, and subsequently dehydrated in 70% ethanol for 30 min, 95% ethanol for 30 min, 3 times in 100% ethanol for 30 min, and 3 times in xylene for 10 min. Following dehydration, tissue samples were incubated in paraffin overnight, and subsequently embedded in paraffin wax.

2.7 Histology

Histology was performed on 3µm formalin fixed paraffin section slides using Hematoxylin and Eosin (H&E) staining. Tissues were deparaffinized and

rehydrated by treatment in xylene for 5 min twice, 100% ethanol for 1 min, 95% ethanol for 1 min, 70% ethanol for 1 min, and in distilled water for 5 min. Harris Modified Method Hematoxylin (Fisher SH26500D) stain was applied for 5 min, washed in distilled water for 5 min. Excess background stain was removed by dipping the silds 8 times in 70% ethanol (containing 0.38% HCl). Hematoxylin stain was chemically converted a blue stain by dipping in 0.1% NH_3OH 8 times. Slides were subsequentially washed in distilled water for 5 min. Eosin Y Phloxine (VWR # 101410-926) was applied for 10 seconds, and slides were dehydrated by 8 dips in 95% ethanol, 8 dips in 100% ethanol, and treated with xylene for 5 min twice. Coverslips were mounted using Permount Mounting Media for H&E (Fisher #SP15-100).

2.8 Immunofluorescence staining

Immunofluorescence (IF) was performed as described on 3µm paraffin sections or 6µm cryosections. Paraffin slides were deparaffinized and rehydrated prior to staining. Slides were washed in PBST 3 times for 5 minutes, and subsequently boiled in Antigen Unmasking Solution (Vector Labs) for 15 minutes, and subsequentially washed with PBST 3 times. Blocking was conducted using 10% Normal Goat Serum diluted in PBS (10% NGS) at room temperature for 1 hour. Primary antibodies (Table 2.7) were diluted in 10% NGS and incubated with samples overnight at 4°C. mCherry antibody was diluted in Normal Horse Serum. Slides were washed with PBST 3 times, incubated with

secondary antibodies diluted (1:600) in 10% NGS for 1 hour at room temperature, and washed with PBST 3 times. Secondary antibodies used: Alexa Fluor 488, 555, or 647 (Invitrogen/Molecular Probes). Coverslips were mounted with mounting medium containing DAPI (Vector Labs H1200) and sealed.

Table 2.1: Primary antibodies used for immunofluorescence staining

Antigen	Supplier	Ig type	Dilution
CK5	Covance #PRB-160P	Rat IgG2a	1:1000
CK18	Abcam #ab668	Rabbit IgG	1:200
GFP	Abcam #13970	Chick IgY	1:4000
E-Cadherin	BD Biosciences #610181	Mouse IgG2a	1:500
Ki67	DakoCytomation #M7249	Rat IgG2a	1:500
Foxa1	Abcam #ab23738	Rabbit IgG	1:2000
mCherry	SICGEN #AB8181-200	Goat IgG	1:500

2.9 Imaging

Whole bladder images and direct GFP visualization were acquired using Nikon SMZ-1000 stereomicroscope with fluorescence and charge-coupled device digital camera. H&E and IF slides were imaged using a Zeiss AxioImager microscope in the UCSC Microscopy Shared Facility.

2.10 Cell dissociation, and deep sequencing

The urothelium was of 12 Cas9 bladders electroporated with sgPTEN-TP53 was excised from the bladder two weeks post-electroporation. The urothelium was digested in DMEM containing 0.25% Trypsin-EDTA (Stemcell Technologies Inc # 07901) and 300U/ml Collagenase B (Sigma #11088807001)

for 1.5 hours at 37°C. Digestion media was deactivated with HBSS (2% FBS) and removed by centrifugation at 350*g for 5 min. 1ml of 5mg/ml Dispase (Stemcell Technologies Inc # 07913) was added and used to dissocate the sample by pipetting for 1 minute. Dispase was deactivated by adding HBSS (2% FBS). Cells were strained through a 40 μm cell strainer, and media was removed by centrifugation at 350*g for 5 min. Then cells were resuspended in HBSS (2% FBS) with EDTA (1.5mM) and sorted for mCherry signal by FACS.

Genomic DNA was isolated from cells and used to amplify TP53 and PTEN sgRNA target loci (using same primers and parameters as section 2.3). PCR amplicons were purified using QIAquick Gel Extraction Kit (QIAGEN # 28506) on a 1% agarose gel. Amplicons were sequenced at UC Davis Genome Center for sequencing using Illumina MiSeq platform (300bp pair-end). Data was processed and analysed by the UC Davis Bioinformatics Core. Sequence variants were determined using FreeBayes, and sequence alignment was conducted using CLUSTAL multiple sequence alignment by MUSCLE (3.8).

Chapter 3: Results

3.1 Development and testing of plasmid delivery by electroporation

To implement the CRISPR/Cas9 system in mice, sgRNA must be introduced into the urothelium. One method to deliver sgRNAs into cells is through the incorporation of the sgRNA into an expression plasmid. There are no established methods for plasmid delivery into the bladder urothelium in vivo. Plasmid delivery using adenovirus in the bladder yields low delivery rates and requires access to biosafety level 2 laboratories (Puzio-Kuter et al., 2009). Experiments using adeno-associated viruses by our lab failed to delivery plasmid into the urothelium. Electroporation is a non-viral technique utilized in vivo for plasmid delivery, and is commonly used *in vivo* in muscles, embryonic mouse brain, and liver (Aihara and Miyazaki, 1998)(Saito and Nakatsuji, 2001) (Heller et al., 1996). The Wang lab developed a novel technique utilizing electroporation to deliver plasmids into the mouse bladder urothelium in vivo. Briefly, this technique involves injecting plasmid directly into the bladder urothelium and electroporating the bladder (Fig 3.1) (Yu et al., 2018).

In order to validate the electroporation technique, determine the efficiency, and characterize the affected cell types, mice bladders were electroporated with pCAG-GFP. Bladders were dissected and analyzed for GFP fluorescence 48 hours post-electroporation. Whole bladders electroplated with

pCAG-GFP exhibited positive GFP signal, compared to the negative control (Fig 3.2a). Immunofluorescence staining for GFP, CK5 (basal and intermediate cell marker), and CK18 (intermediate and umbrella cell marker) indicate GFP signal in all three cell types. No GFP signal is present in the muscle layer (Fig 3.2b). Approximately 15% of the urothelial cells exhibited positive GFP signal. Positive GFP signal was present 7- and 14-days post-electroporation (Fig 3.2c and d). Delivery of multiple plasmids was investigated by co-electroporation of CFP and mCherry plasmids. CFP is expressed in 72% of mCherry postive cells (Fig 3.3).

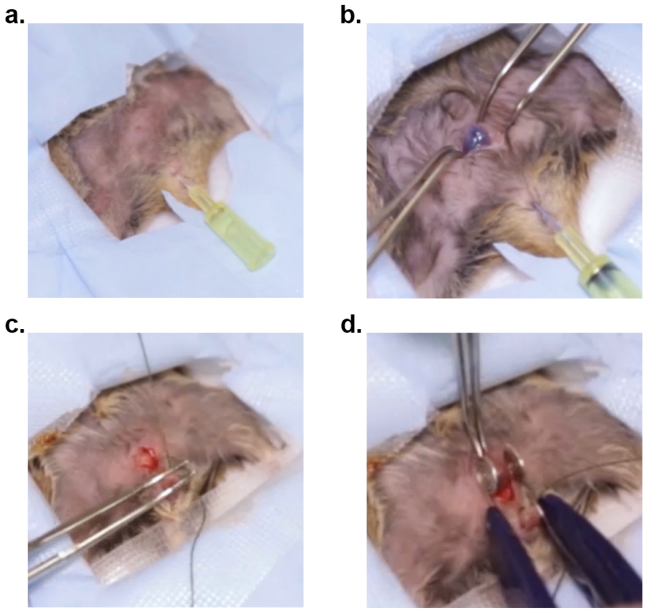

Figure 3.1: Bladder urothelium electroporation technique.
Images from Yu et al. video demonstrating bladder electroporation depicting major steps: bladder catheterization (a), plasmid injection into the bladder lumen (b), tying of the urethral orifice to prevent plasmid backflow (c), and electroporation of the bladder (d).

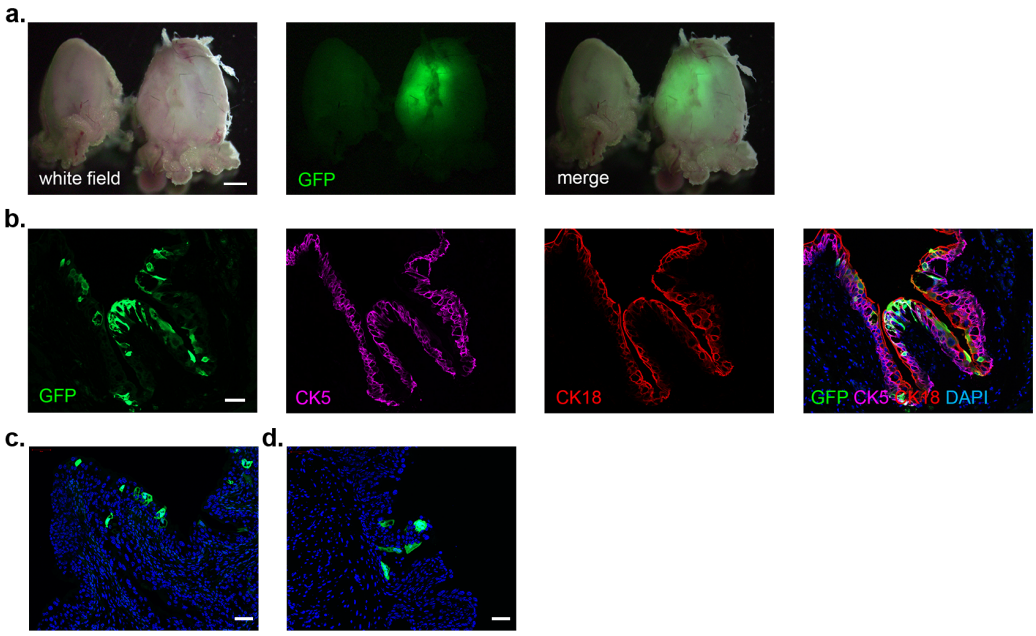

Figure 3.2: Electroporation successfully delivers plasmids into mouse bladder urothelium

a) Whole mouse bladders unelectroporated control (left) and electroporated with GFP plasmid (right) shown in brightfield and direct GFP visualization. b) Sections of GFP electroporated bladder IF stained for GFP, CK5, CK18, and DAPI. Sections of bladder electroporated with GFP plasmid analyzed 7- (c) or 14-days (d) post-electroporation using direct GFP visualization and DAPI. Scale bar corresponds to 1 mm in (a) and 50 μm in (b, c, and d). (a, and b) are from Yu et al. 2018

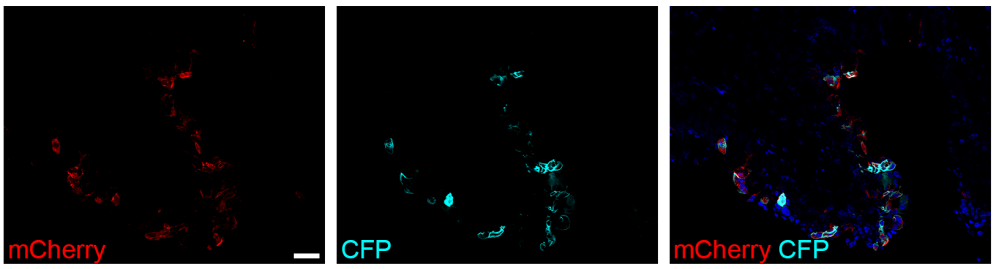

Figure 3.3: Co-electroporation of plasmids **into the bladder urothelium.** Sections of bladder co-electroporated with mCherry and CFP plasmids. Florescence analyzed by direct visualization of mCherry and CFP. Nuclei stained with DAPI. Scale bar corresponds to 50 μm.

3.2 Design and validation TP53 and PTEN sgRNA plasmid

Mutations to common tumor suppressor genes TP53 and PTEN, using Cre-LoxP were shown to induce MIBC in mice (Puzio-Kuter et al., 2009). In order to recapitulate this phenotype using CRISPR/Cas9 by electroporation, sgRNAs targeting PTEN and TP53 (hereafter termed sgPTEN and sgTP53, respectively) were cloned into a mCherry plasmid and validated. The sgTP53 and sgPTEN sequences utilized in this study were previously used *in vivo* liver cancer models (Xue et al., 2014). The sgRNAs were initially validated for mutation at the targeted loci. NIH/3T3 cells were transfected with Cas9 expression plasmid containing sgTP53 or sgPTEN. Genomic DNA was amplified at the targeted loci, and the Surveyor Assay was used to analyze for mutations. Cells transfected with sgTP53 or sgPTEN incurred indels indicated by the presence of bands compared to wildtype cells (Fig 3.4).

For plasmid delivery by electroporation sgTP53 and sgPTEN were cloned into an mCherry vector, under the expression of a mouse and human U6 promoters, respectively (plasmid hereafter termed sgPTEN-TP53) (Fig 3.5a). To determine if sgPTEN-TP53 properly cuts at PTEN and TP53 loci, NIH3T3 cells were co-transfected with sgPTEN-TP53 and Cas9 expression plasmids, sgRNA target sites were amplified and analyzed by sequencing. Sequencing results indicated the presence of mismatches around the TP53 and PTEN target cut site locus, as noted in the presence of different peaks (Fig. 3.5b).

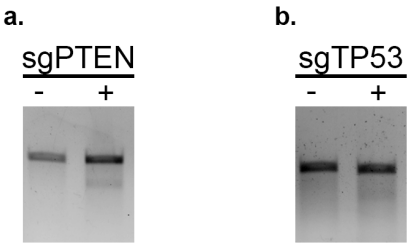

Figure 3.4: Validation of sgPTEN and sgTP53 *in vitro*.
Validation of sgPTEN (a) or sgTP53 (b) using the Surveyor Assay. NIH/3T3 cells were transfected (+, experimental) or not transfected (-, control) with plasmid a pX330 containing sgPTEN or sgTP53. Surveyor assay was conducted on PCR amplicons of the target loci. (a) sgPTEN target amplicon is 413 bp and present in both control and experimental samples. sgPTEN Surveyor product is 303 bp in experimental sample. (b) sgTP53 target amplicons is 331 bp present in both control and experimental samples. sgTP53 product is 229 bp in the experimental sample. Samples were run 1% agarose gel. Gel images were cropped due presence of unrelated samples.

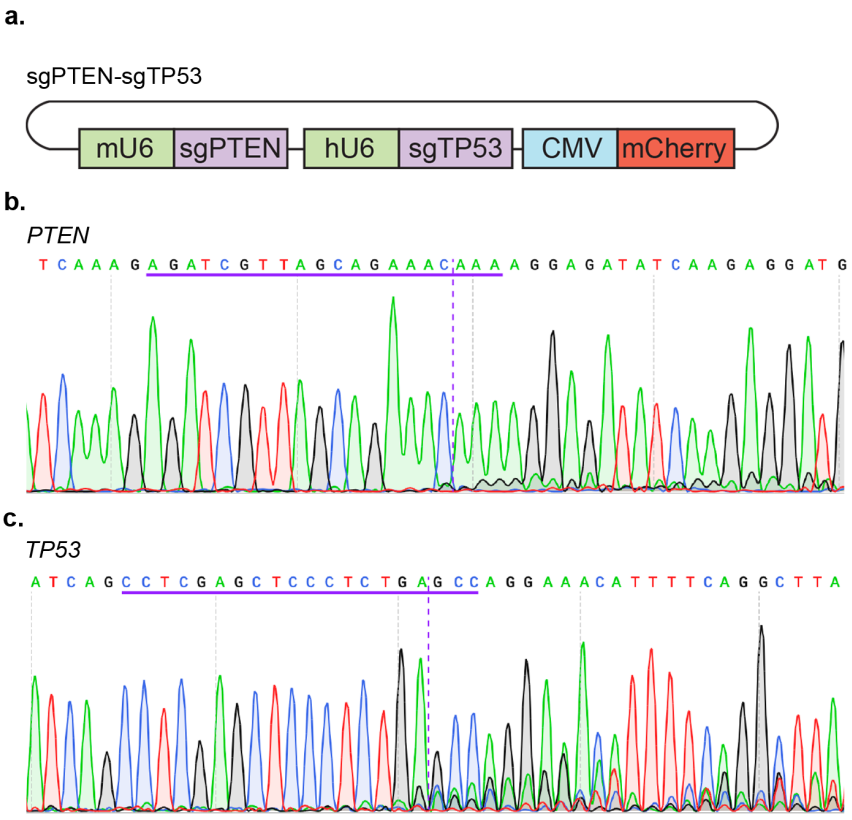

Figure 3.5: Validation of sgPTEN-TP53 plasmid *in vitro.*
a) Diagram of the sgPTEN-TP53 plasmid. sgRNAs targeting PTEN and TP53 were cloned into a mCherry plasmid under the expression of mouse U6 (mU6) and human U6 (hU6) promoters, respectively. b) Sanger sequencing results of sgRNA target locus amplicons generated by transfection of NIH/3T3 cells with sgPTEN-TP53 and Cas9 plasmid. sgRNA sequence is underlined in purple, and a dashed line indicts the expected Cas9 cut site.

3.3 *In vivo* validation of sgPTEN-TP53

To determine if sgPTEN-TP53 induces mutations in vivo, deep sequencing was performed on sgRNA target amplicons generated from sgPTEN-TP53 electroporated Cas9 urothelial cells. Urothelial cells were collected 2 weeks post-electroporation with sgPTEN-TP53, and amplicons were generated for the

PTEN and TP53 sgRNA target loci. Examples of mutations caused by sgPTEN-TP53 on TP53 and PTEN target locus are shown in Figures 3.6a and b**,** respectively. Indel mutation analysis reveals that the majority of the mutations at the TP53 locus induce frameshifts (deletions of 1,2,4,5,7, or 8 and insertions of 1, or 2 nucleotides). Large deletions (>9 nucleotides) were also observed.

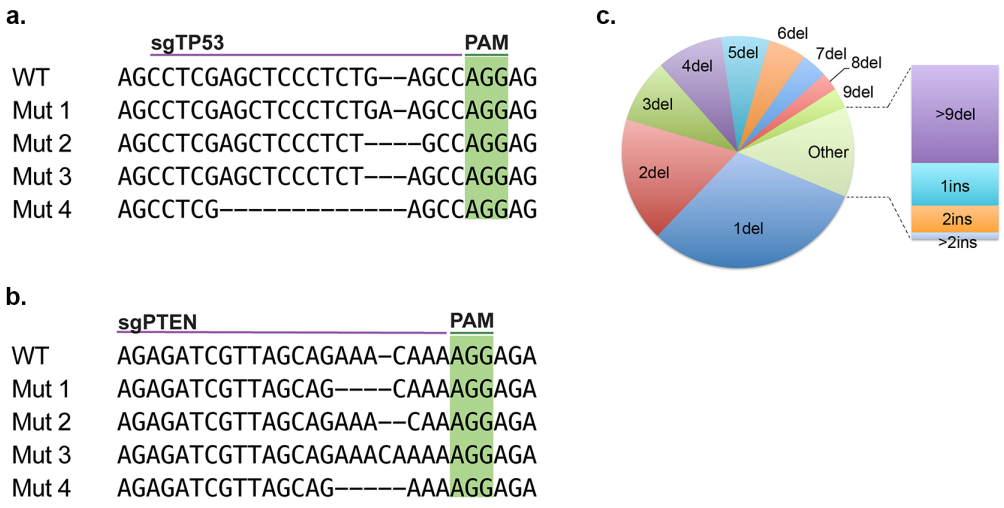

Figure 3.6: *In vivo* sgPTEN-TP53 mutation analysis.
a) and b) Example of mutations determined by sequencing of TP53 and PTEN sgRNA target loci amplicons, respectively. Positive mCherry urothelial cells were sorted by FACS from 12 Cas9 mouse bladders electroporated with sgPTEN-TP53 2 weeks post-electroporation. c) Indel size analysis for TP53 sgRNA target locus. Alignment by CLUSTAL multiple sequence alignment by MUSCLE (3.8)

3.4 CRISPR/Cas9 mutation induces tumors in the bladder

To determine if CRISPR/Cas9 can be used to induce BCa tumors in vivo, Cas9 mice were electroporated with sgPTEN-TP53 and histologically analyzed at 3, 6, or 12 months post-electroporation. For control, Cas9 mice were electroporated with an empty mCherry vector or were not electroporated. The Cas9 mouse strain was validated for Cas9 expression in the urothelium by the expression of the GFP reporter (Fig. 3.7a)(Platt et al., 2014). Electroporation of sgPTEN-TP53 was validated by IF staining for mCherry, 2 weeks post-electroporation (Fig 3.7b). Both mCherry electroporated and not electroporated bladder were histologically identical and displayed a normal urothelium. Non-pathologically significant lymphocyte infiltration were present in the control mice (Fig. 3.8a, b) (Frazier et al., 2012).

Experimental sgPTEN-TP53 revealed no phenotypic changes after 3- or 6- months (n=6 for each time point) post-electroporation (Fig 3.9a, b). Lymphocyte infiltration was observed at 6- and 12- month time points. 12 months post-electroporation, 2 bladders electroporated with sgPTEN-TP53 (n=6) exhibited increased urothelial layer indicating a tumor phenotype (Fig 3.9c, d). The tumors were phenotypically different. The tumor in Figure 3.4c exhibited growth into the lumen and characteristics of carcinomas: irregularity in cell size, loss of cell polarity, and nuclear pleomorphisms. The tumor in Figure 3.4d exhibited an increase of the urothelial layer and resembles hyperplasia (Mostofi et al., 1973)(Montironi and Lopez-Beltran, 2005) (Humphrey et al., 2016).

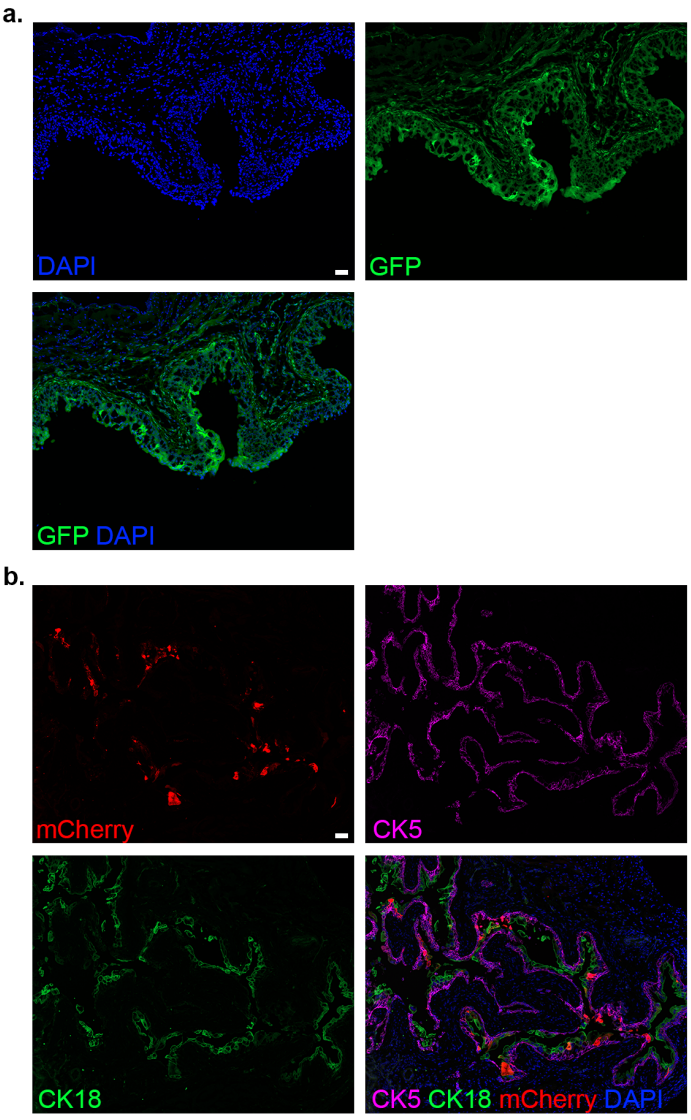

Figure 3.7: Validation of Cas9 expression and sgPTEN-TP53 electroporation in the urothelium.
a) Bladder urothelium section of Cas9 mice, direct GFP visualization reports expression of Cas9. b) Bladder urothelium of Cas9 mouse 2 weeks post-electroporation with sgPTEN-TP53, IF stained for mCherry, CK5, CK18. Nuclei are shown using DAPI. Scale bar corresponds to 50 μm.

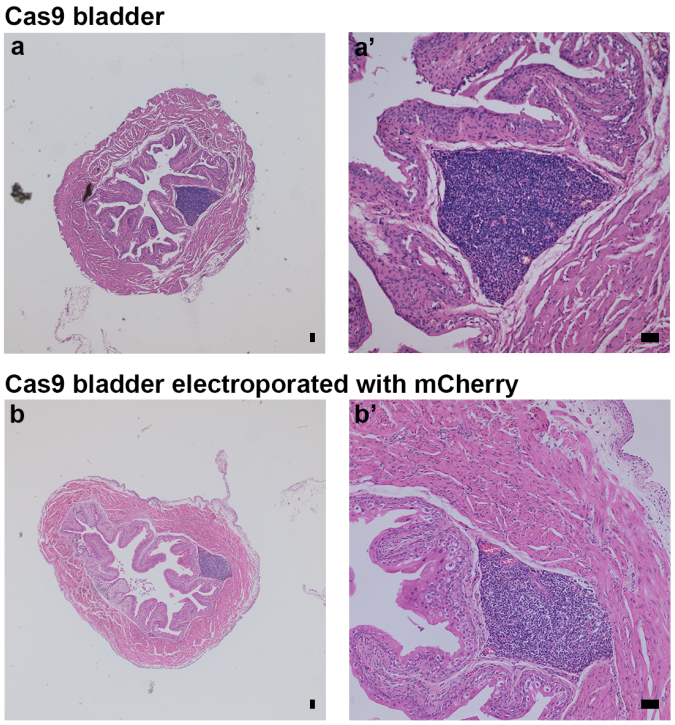

Figure 3.8: Histology of control Cas9 bladders.
Representative histological images of a) Cas9 bladder sections electroporated with mCherry control plasmid analyzed 6 months post-electroporation and b) 9-month-old Cas9 mouse bladder sections not electroporated. Both bladders exhibit lymphocytic aggregates. Scale bars corresponds to 50 μm.

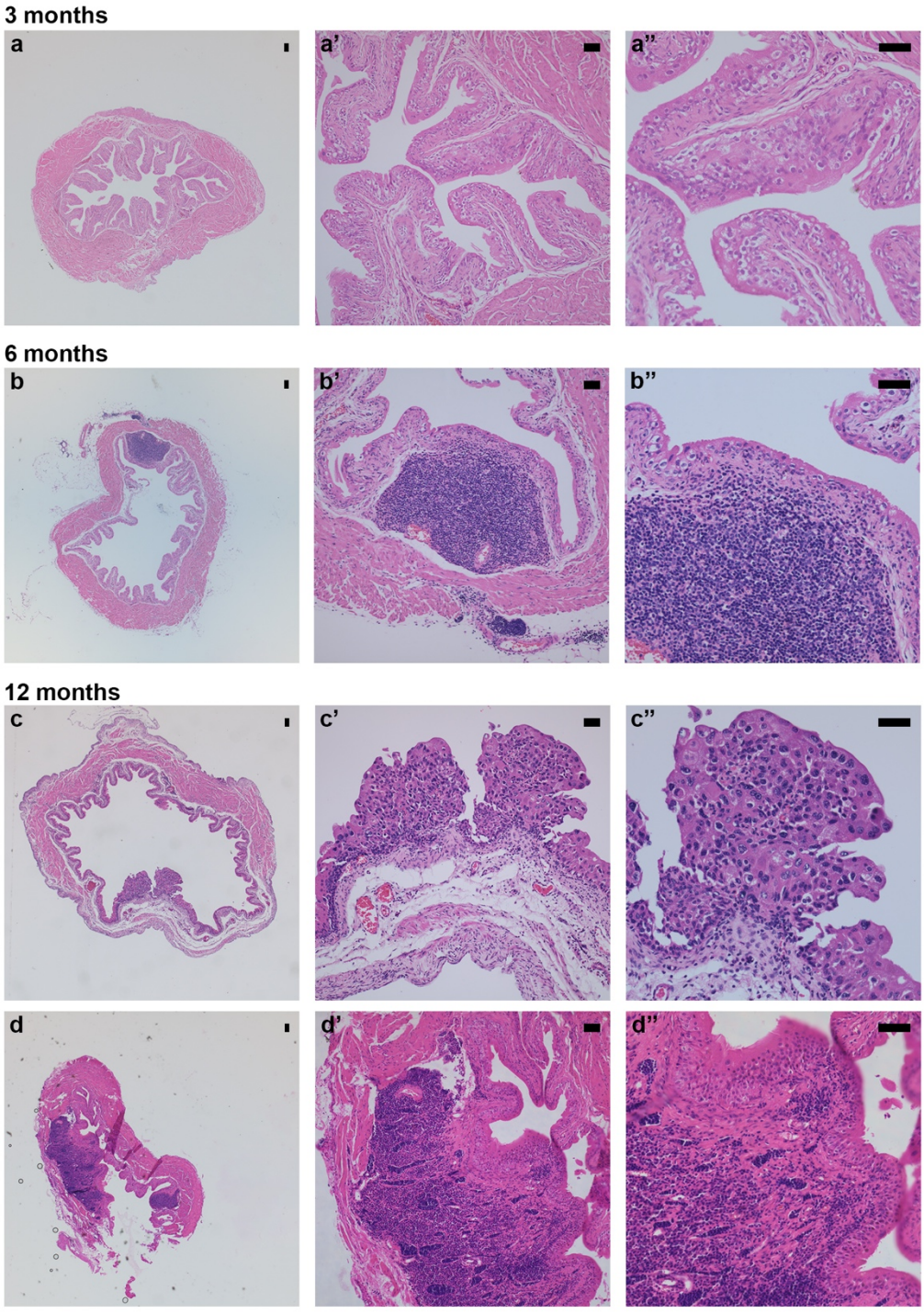

Figure 3.9: Histology of bladders electroporated with of sgRNAs targeting TP53 and PTEN.

(Figure 3.9 continued) Histological analysis of Cas9 bladder sections electroporated with sgPTEN-TP53 3- (a), 6- (b), and 12- months (c, d) post-electroporation (n=6 for each time point). (a, b) are representative images from the entire cohort. (c, d) Represent 2 different mice bladders. Tumor in (c) resembles carcinoma phenotype, and (d) resembles hyperplasia. Scale bar corresponds to 50 μm.

3.5 Pathology of CRISPR/Cas9 induced bladder tumors

Immunofluorescent (IF) staining was used to characterize the pathology of the electroporated bladders. The histologically identified tumors were analyzed for epithelial markers. The mouse bladder is expected to have a single layer of Umbrella cells (CK18 positive), a single layer of intermediate cells (CK5 positive), and two layers of intermediate cells (lower levels of CK5, and CK18), as observed in wildtype bladders (3.10). Bladders identified with a tumor phenotype exhibited an increased in the CK5 layer, compared to wild type regions (Fig. 3.11a and 3.12a). Only a single layer of CK18 is present in the tumor region (Fig. 3.11a). E-cadherin is an epithelial cell surface marker and normally expressed in the urothelium, and loss of E-cadherin is associated increased tumor aggression (Shorning et al., 2011). E-cadherin was expressed in the urothelium of both tumors (Fig 3.11a, and 3.12b). Foxa1 is an epithelial transcription regulator and expected to be expressed in all urothelial cells. Decreased Foxa1 expression associated with basal/squamous MIBC subtype (Osei-Amponsa et al., 2019). Foxa1 expression is found in the tumor region (Fig 3.11c).

Ki67 marks cells undergoing proliferation and used for cancer diagnoses (Scholzen and Gerdes, 2000). Bladders were IF stained for Ki67, and Ki67 index was quantified. The wildtype mouse urothelium is quiescent, and low positive Ki67 staining is expected (Jaal and Dörr, 2010) (Stewart et al., 1980). Control mice exhibited an average of 0.32% Ki67 positive nuclei (Fig 3.10a). The tumor histologically resembling carcinoma exhibited 13% Ki67 positive nuclei (Fig 3.11a). In comparison, the tumor histologically resembling hyperplasia exhibited 0.55% Ki66 positive nuclei (Fig 12a).

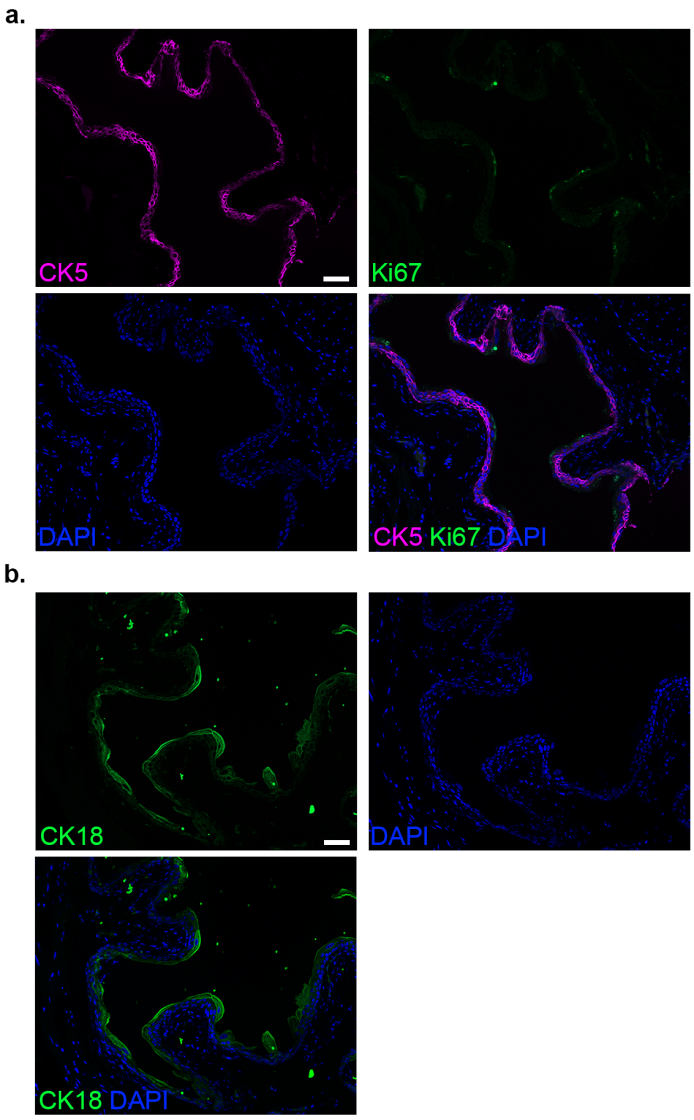

Figure 3.10: Pathology of control Cas9 bladders.
Representative images of 6-month-old Cas9 bladder sections immunofluorescent stained for a) CK5, Ki67 b) CK18. Nuclei stained with DAPI. Scale bars corresponds to 50 μm.

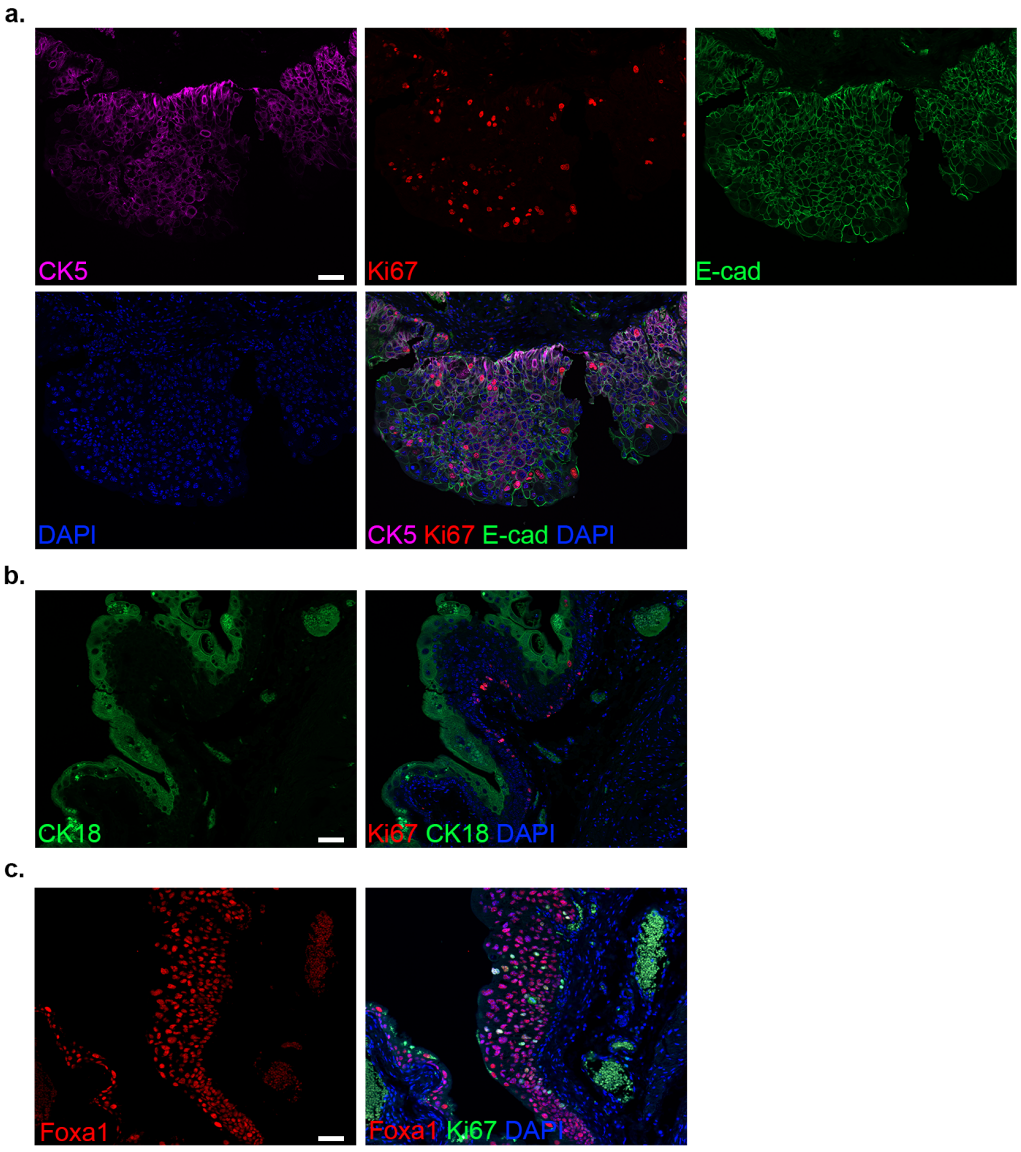

Figure 3.11: Increased cell proliferation and basal cell layer due to sgPTEN-TP53 in tumor resembling carcinoma.
Cas9 mouse bladder sections electroporated with sgPTEN-TP53 analyzed pathologically analyzed 12-months post electroporation by IF staining for a) CK5, E-cadherin (E-cad), and Ki67. b) CK18, Ki67. c) Foxa1, Ki67. Sections are adjacent to bladder sections from Figure 3.4c. Nuclei stained with DAPI. Scale bars corresponds to 50 μm.

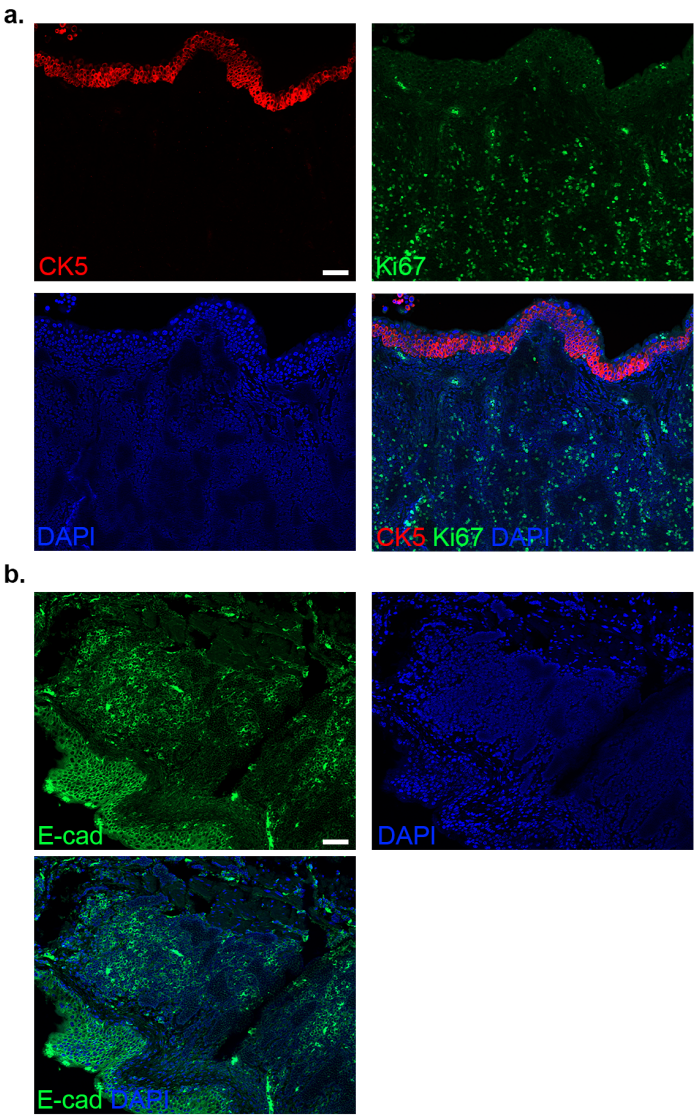

Figure 3.12: sgPTEN-TP53 induced an increase in the CK5 basal cell layer. Pathological analysis of Cas9 bladder electroporated with sgPTEN-TP53 analyzed 12 months post-electroporation with tumor remembering hyperplasia IF stained for a) CK5, Ki67 b) E-cadherin (E-cad). Nuclei stained with DAPI. Sections are adjacent to bladder sections from Figure 3.4d. Scale bars corresponds to 50 μm.

Chapter 4: Discussion

Recent sequencing studies identified frequently mutated genes in BCa; however, it is unknown how many of these mutations impact BCa pathogenesis (Robertson et al., 2017)(Pietzak et al., 2017). Current in vivo Cre-LoxP models are inefficient studying BCa disease pathogenesis due to the time and expense required to generated floxed mice for mutated genes, and also depend on available flox genes (Kobayashi et al., 2015). This project described a novel method overcome those hurdles by utilizing CRISPR/Cas9, by which plasmids containing sgRNAs are delivered to the mouse urothelium by electroporation.

This study demonstrated the feasibility of DNA plasmid delivery into the mouse urothelium by electroporation. Electroporation of mCherry and GFP expression plasmids into the urothelium was shown, and the fluorescence signal was observed for at least 2 weeks post-electroporation. Furthermore, this technique can be utilized to deliver multiple plasmids into the urothelium. This non-viral approach provides the field with a new tool for DNA delivery to the urothelium and can be used in lieu of adenovirus for Cre delivery into the urothelium.

As a proof-of-principle experiment on the utilization of CRISPR/Cas9 to investigate bladder carcinogenesis, a plasmid containing sgRNAs targeting PTEN and TP53 was electroporated into the bladder of Cas9 mice to recapitulate an established BCa model. Overall, two tumors were observed (33% efficiency).

These tumors are characterized as hyperplasia and low-grade papillary tumors. However, these phenotypes need to be validated by a pathologist. Notably, both tumors exhibited an increase of the CK5 layer, suggesting a basal or intermediate cell of origin, but due to plasmid penetrance into all urothelial cell types, it is difficult to infer the cell of origin. Experiments using lineage tracing are required to determine the cell of origin.

The CRISPR/Cas9 model is not as efficient as the PTEN and TP53 the Cre-LoxP models described. Adenovirus delivery of Cre induced tumors at 100% penetrance by 6 months post-infection and resulted in invasive and metastatic phenotypes (Puzio-Kuter et al., 2009). The UP3a-CreERT2 knockout model resulted in 95% efficiency by 77 weeks with similar phenotypes to the adenovirus model (Saito et al., 2018).

Differences between Cre-LoxP and CRISPR/Cas9 are due to the underlying biology behind those techniques. Cre-LoxP knockout excises a large gene segment by recombination, ensuring complete deactivation of genes. In contrast, CRISPR/Cas9 induced mutations depend on the NHEJ mechanism leading to heterogenous indel mutations (mosaic mutations), potentially not inducing biallelic inactivation of *TP53* and *PTEN*. Importantly, Puzio-Kuter et al. observed that biallelic knockout both *TP53* and *PTEN* is required for bladder carcinogenesis. Further, mosaicism challenges tumor comparisons and requires sequencing to gain biological insight. Overcoming the hurdles of CRISPR/Cas9 is

beneficial as this technique would dramatically reduce the cost and time for bladder cancer modeling.

One approach to reduce CRISPR/Cas9 mutational variability is gene inactivation at the transcriptional level using CRISPR interference (CRISPRi). This technique utilizes an endonuclease inactive or dead Cas9 (dCas9), which maintains its genomic targeting function. dCas9 can be used block transcription initiation or elongation by design of sgRNAs targeting promoter or the target gene, respectively (Qi et al., 2013). CRISPRi was used to induce lymphoma in immunocompromised mice by transplantation of lymphocytes silenced for *TP53* using dCas9 (Braun et al., 2016). However, direct *in vivo* CRISPRi models have yet to be established.

In conclusion, this work demonstrated the feasibility of using CRISPR/Cas9 to model BCa *in vivo*, accomplished but the delivery of sgRNA expression plasmids by electroporation into the bladder of Cas9 expressing mice. This technique used to study the effects of other genes on BCa *in vivo* but requires optimization to improve tumor penetrance.

Appendix

Full sgPTEN-TP53 insert sequence.

Sequence inserted into AseI restriction site in mCherry-C2 (Addgene # 54563) to construct sgPTEN-TP53 for electroporation expreriment. Sequence contains mouse U6 promoter, *PTEN* sgRNA and scaffold, spacer sequence, human U6 promoter, *TP53* sgRNA and scaffold.

5’- GATCCGACGCCGCCATCTCTAGGCCCGCGCCGGCCCCCTCGCACAG
ACTTGTGGGAGAAGCTCGGCTACTCCCCTGCCCCGGTTAATTTGCATA
TAATATTTCCTAGTAACTATAGAGGCTTAATGTGCGATAAAAGACAGA
TAATCTGTTCTTTTTAATACTAGCTACATTTTACATGATAGGCTTGGAT
TTCTATAAGAGATACAAATACTAAATTATTATTTTAAAAAACAGCACA
AAAGGAAACTCACCCTAACTGTAAAGTAATTGTGTGTTTTGAGACTAT
AAATATCCCTTGGAGAAAAGCCTTGTTGAAACACCGAGATCGTTAGCA
GAAACAAAGTTTTAGAGCTAGAAATAGCAAGTTAAAATAAGGCTAGT
CCGTTATCAACTTGAAAAAGTGGCACCGAGTCGGTGCTTTTTTTAGCC
GAACTGTTTCACACTCACGCGTCCAAGGTCGGGCAGGAAGAGGGCCT
ATTTCCCATGATTCCTTCATATTTGCATATACGATACAAGGCTGTTAGA
GAGATAATTGGAATTAATTTGACTGTAAACACAAAGATATTAGTACAA
AATACGTGACGTAGAAAGTAATAATTTCTTGGGTAGTTTGCAGTTTTA
AAATTATGTTTTAAAATGGACTATCATATGCTTACCGTAACTTGAAAG
TATTTCGATTTCTTGGCTTTATATATCTTGTGGAAAGGACGAAACACCG
CCTCGAGCTCCCTCTGAGCCGTTTTAGAGCTAGAAATAGCAAGTTAAA
ATAAGGCTAGTCCGTTATCAACTTGAAAAAGTGGCACCGAGTCGGTGC
TTTTTTTGGATCCAATTCTACC -3’

References

Ahmad, I., Singh, L.B., Foth, M., Morris, C.-A., Taketo, M.M., Wu, X.-R., Leung, H.Y., Sansom, O.J., Iwata, T., 2011. K-Ras and -catenin mutations cooperate with Fgfr3 mutations in mice to promote tumorigenesis in the skin and lung, but not in the bladder. Dis. Model. Mech. 4, 548–555. https://doi.org/10.1242/dmm.006874

Aihara, H., Miyazaki, J., 1998. Gene transfer into muscle by electroporation in vivo. Nat. Biotechnol. 16, 867–870. https://doi.org/10.1038/nbt0998-867

Allory, Y., Beukers, W., Sagrera, A., Flández, M., Marqués, M., Márquez, M., van der Keur, K.A., Dyrskjot, L., Lurkin, I., Vermeij, M., Carrato, A., Lloreta, J., Lorente, J.A., Carrillo-de Santa Pau, E., Masius, R.G., Kogevinas, M., Steyerberg, E.W., van Tilborg, A.A.G., Abas, C., Orntoft, T.F., Zuiverloon, T.C.M., Malats, N., Zwarthoff, E.C., Real, F.X., 2014. Telomerase Reverse Transcriptase Promoter Mutations in Bladder Cancer: High Frequency Across Stages, Detection in Urine, and Lack of Association with Outcome. Eur. Urol. 65, 360–366. https://doi.org/10.1016/j.eururo.2013.08.052

Braun, C.J., Bruno, P.M., Horlbeck, M.A., Gilbert, L.A., Weissman, J.S., Hemann, M.T., 2016. Versatile in vivo regulation of tumor phenotypes by dCas9-mediated transcriptional perturbation. Proc. Natl. Acad. Sci. 113, E3892–E3900. https://doi.org/10.1073/pnas.1600582113

Choi, W., Porten, S., Kim, S., Willis, D., Plimack, E.R., Hoffman-Censits, J., Roth, B., Cheng, T., Tran, M., Lee, I.-L., Melquist, J., Bondaruk, J., Majewski, T., Zhang, S., Pretzsch, S., Baggerly, K., Siefker-Radtke, A., Czerniak, B., Dinney, C.P.N., McConkey, D.J., 2014. Identification of Distinct Basal and Luminal Subtypes of Muscle-Invasive Bladder Cancer with Different Sensitivities to Frontline Chemotherapy. Cancer Cell 25, 152–165. https://doi.org/10.1016/j.ccr.2014.01.009

Clayson, D.B., Fishbein, L., Cohen, S.M., 1995. Effects of stones and other physical factors on the induction of rodent bladder cancer. Food Chem. Toxicol. 33, 771–784. https://doi.org/10.1016/0278-6915(95)00044-3

Colopy, S.A., Bjorling, D.E., Mulligan, W.A., Bushman, W., 2014. A population of progenitor cells in the basal and intermediate layers of the murine bladder urothelium contributes to urothelial development and regeneration: Urothelial Development and Regeneration. Dev. Dyn. 243, 988–998. https://doi.org/10.1002/dvdy.24143

Dahm, P., Gschwend, J.E., 2003. Malignant Non-Urothelial Neoplasms of the Urinary Bladder: A Review. Eur. Urol. 44, 672–681. https://doi.org/10.1016/S0302-2838(03)00416-0

Das, G., Henning, D., Wright, D., Reddy, R., 1988. Upstream regulatory elements are necessary and sufficient for transcription of a U6 RNA gene by RNA polymerase III. EMBO J. 7, 503–512.

di Martino, E., L'Hôte, C.G., Kennedy, W., Tomlinson, D.C., Knowles, M.A., 2009. Mutant fibroblast growth factor receptor 3 induces intracellular signaling and cellular transformation in a cell type- and mutation-specific manner. Oncogene 28, 4306–4316. https://doi.org/10.1038/onc.2009.280

Foth, M., Ahmad, I., van Rhijn, B.W., van der Kwast, T., Bergman, A.M., King, L., Ridgway, R., Leung, H.Y., Fraser, S., Sansom, O.J., Iwata, T., 2014. Fibroblast growth factor receptor 3 activation plays a causative role in urothelial cancer pathogenesis in cooperation with *Pten* loss in mice: Functional role of FGFR3 in urothelial cancer. J. Pathol. 233, 148–158. https://doi.org/10.1002/path.4334

Frazier, K.S., Seely, J.C., Hard, G.C., Betton, G., Burnett, R., Nakatsuji, S., Nishikawa, A., Durchfeld-Meyer, B., Bube, A., 2012. Proliferative and Nonproliferative Lesions of the Rat and Mouse Urinary System. Toxicol. Pathol. 40, 14S-86S. https://doi.org/10.1177/0192623312438736

Hartmann, A., Schlake, G., Zaak, D., Hungerhuber, E., Hofstetter, A., Hofstaedter, F., Knuechel, R., 2002. Occurrence of chromosome 9 and p53 alterations in multifocal dysplasia and carcinoma in situ of human urinary bladder. Cancer Res. 62, 809–818.

He, F., Melamed, J., Tang, M. -s., Huang, C., Wu, X.-R., 2015. Oncogenic HRAS Activates Epithelial-to-Mesenchymal Transition and Confers Stemness to p53-Deficient Urothelial Cells to Drive Muscle Invasion of Basal Subtype

Carcinomas. Cancer Res. 75, 2017–2028. https://doi.org/10.1158/0008-5472.CAN-14-3067

He, F., Mo, L., Zheng, X.-Y., Hu, C., Lepor, H., Lee, E.Y.-H.P., Sun, T.-T., Wu, X.-R., 2009. Deficiency of pRb Family Proteins and p53 in Invasive Urothelial Tumorigenesis. Cancer Res. 69, 9413–9421. https://doi.org/10.1158/0008-5472.CAN-09-2158

Hedegaard, J., Lamy, P., Nordentoft, I., Algaba, F., Høyer, S., Ulhøi, B.P., Vang, S., Reinert, T., Hermann, G.G., Mogensen, K., Thomsen, M.B.H., Nielsen, M.M., Marquez, M., Segersten, U., Aine, M., Höglund, M., Birkenkamp-Demtröder, K., Fristrup, N., Borre, M., Hartmann, A., Stöhr, R., Wach, S., Keck, B., Seitz, A.K., Nawroth, R., Maurer, T., Tulic, C., Simic, T., Junker, K., Horstmann, M., Harving, N., Petersen, A.C., Calle, M.L., Steyerberg, E.W., Beukers, W., van Kessel, K.E.M., Jensen, J.B., Pedersen, J.S., Malmström, P.-U., Malats, N., Real, F.X., Zwarthoff, E.C., Ørntoft, T.F., Dyrskjøt, L., 2016. Comprehensive Transcriptional Analysis of Early-Stage Urothelial Carcinoma. Cancer Cell 30, 27–42. https://doi.org/10.1016/j.ccell.2016.05.004

Heller, R., Jaroszeski, M., Atkin, A., Moradpour, D., Gilbert, R., Wands, J., Nicolau, C., 1996. In vivo gene electroinjection and expression in rat liver. FEBS Lett. 389, 225–228. https://doi.org/10.1016/0014-5793(96)00590-X

Hicks, R.M., 1975. THE MAMMALIAN URINARY BLADDERAN ACCOMMODATING ORGAN. Biol. Rev. 50, 215–246. https://doi.org/10.1111/j.1469-185X.1975.tb01057.x

Hopman, A.H.N., Kamps, M.A.F., Speel, E.J.M., Schapers, R.F.M., Sauter, G., Ramaekers, F.C.S., 2002. Identification of Chromosome 9 Alterations and p53 Accumulation in Isolated Carcinoma in Situ of the Urinary Bladder versus Carcinoma in Situ Associated with Carcinoma. Am. J. Pathol. 161, 1119–1125. https://doi.org/10.1016/S0002-9440(10)64388-X

Hu, P., Deng, F.-M., Liang, F.-X., Hu, C.-M., Auerbach, A.B., Shapiro, E., Wu, X.-R., Kachar, B., Sun, T.-T., 2000. Ablation of Uroplakin III Gene Results in Small Urothelial Plaques, Urothelial Leakage, and Vesicoureteral Reflux. J. Cell Biol. 151, 961–972. https://doi.org/10.1083/jcb.151.5.961

Humphrey, P.A., Moch, H., Cubilla, A.L., Ulbright, T.M., Reuter, V.E., 2016. The 2016 WHO Classification of Tumours of the Urinary System and Male Genital Organs—Part B: Prostate and Bladder Tumours. Eur. Urol. 70, 106–119. https://doi.org/10.1016/j.eururo.2016.02.028

Hurst, C.D., Platt, F.M., Taylor, C.F., Knowles, M.A., 2012. Novel Tumor Subgroups of Urothelial Carcinoma of the Bladder Defined by Integrated Genomic Analysis. Clin. Cancer Res. 18, 5865–5877. https://doi.org/10.1158/1078-0432.CCR-12-1807

Iyer, G., Al-Ahmadie, H., Schultz, N., Hanrahan, A.J., Ostrovnaya, I., Balar, A.V., Kim, P.H., Lin, O., Weinhold, N., Sander, C., Zabor, E.C., Janakiraman, M., Garcia-Grossman, I.R., Heguy, A., Viale, A., Bochner, B.H., Reuter, V.E., Bajorin, D.F., Milowsky, M.I., Taylor, B.S., Solit, D.B., 2013. Prevalence and Co-Occurrence of Actionable Genomic Alterations in High-Grade Bladder Cancer. J. Clin. Oncol. 31, 3133–3140. https://doi.org/10.1200/JCO.2012.46.5740

Jaal, J., Dörr, W., 2010. Radiation Effects on Cellularity, Proliferation and EGFR Expression in Mouse Bladder Urothelium. Radiat. Res. 173, 479–485. https://doi.org/10.1667/RR1759.1

Jost, S.P., Gosling, J.A., Dixon, J.S., 1989. The morphology of normal human bladder urothelium. J. Anat. 167, 103–115.

Jost, S.P., Potten, C.S., 1986. Urothelial Proliferation In Growing Mice. Cell Prolif. 19, 155–160. https://doi.org/10.1111/j.1365-2184.1986.tb00725.x

Kamat, A.M., Hahn, N.M., Efstathiou, J.A., Lerner, S.P., Malmström, P.-U., Choi, W., Guo, C.C., Lotan, Y., Kassouf, W., 2016. Bladder cancer. The Lancet 388, 2796–2810. https://doi.org/10.1016/S0140-6736(16)30512-8

Kamoun, A., de Reyniès, A., Allory, Y., Sjödahl, G., Robertson, A.G., Seiler, R., Hoadley, K.A., Groeneveld, C.S., Al-Ahmadie, H., Choi, W., Castro, M.A.A., Fontugne, J., Eriksson, P., Mo, Q., Kardos, J., Zlotta, A., Hartmann, A., Dinney, C.P., Bellmunt, J., Powles, T., Malats, N., Chan, K.S., Kim, W.Y., McConkey, D.J., Black, P.C., Dyrskjøt, L., Höglund, M., Lerner, S.P., Real, F.X., Radvanyi, F., 2019. A Consensus Molecular

Classification of Muscle-invasive Bladder Cancer. Eur. Urol. S0302283819306955. https://doi.org/10.1016/j.eururo.2019.09.006

Khandelwal, P., Abraham, S.N., Apodaca, G., 2009. Cell biology and physiology of the uroepithelium. Am. J. Physiol.-Ren. Physiol. 297, F1477–F1501. https://doi.org/10.1152/ajprenal.00327.2009

Kobayashi, T., Owczarek, T.B., McKiernan, J.M., Abate-Shen, C., 2015. Modelling bladder cancer in mice: opportunities and challenges. Nat. Rev. Cancer 15, 42–54. https://doi.org/10.1038/nrc3858

Kong, X.-T., Deng, F.-M., Hu, P., Liang, F.-X., Zhou, G., Auerbach, A.B., Genieser, N., Nelson, P.K., Robbins, E.S., Shapiro, E., Kachar, B., Sun, T.-T., 2004. Roles of uroplakins in plaque formation, umbrella cell enlargement, and urinary tract diseases. J. Cell Biol. 167, 1195–1204. https://doi.org/10.1083/jcb.200406025

Kunkel, G.R., Maser, R.L., Calvet, J.P., Pederson, T., 1986. U6 small nuclear RNA is transcribed by RNA polymerase III. Proc. Natl. Acad. Sci. 83, 8575–8579. https://doi.org/10.1073/pnas.83.22.8575

Lavelle, J., Meyers, S., Ramage, R., Bastacky, S., Doty, D., Apodaca, G., Zeidel, M.L., 2002. Bladder permeability barrier: recovery from selective injury of surface epithelial cells. Am. J. Physiol.-Ren. Physiol. 283, F242–F253. https://doi.org/10.1152/ajprenal.00307.2001

Lindgren, D., Liedberg, F., Andersson, A., Chebil, G., Gudjonsson, S., Borg, Å., Månsson, W., Fioretos, T., Höglund, M., 2006. Molecular characterization of early-stage bladder carcinomas by expression profiles, FGFR3 mutation status, and loss of 9q. Oncogene 25, 2685–2696. https://doi.org/10.1038/sj.onc.1209249

López-Knowles, E., Hernández, S., Malats, N., Kogevinas, M., Lloreta, J., Carrato, A., Tardón, A., Serra, C., Real, F.X., 2006. *PIK3CA* Mutations Are an Early Genetic Alteration Associated with *FGFR3* Mutations in Superficial Papillary Bladder Tumors. Cancer Res. 66, 7401–7404. https://doi.org/10.1158/0008-5472.CAN-06-1182

Maresch, R., Mueller, S., Veltkamp, C., Öllinger, R., Friedrich, M., Heid, I., Steiger, K., Weber, J., Engleitner, T., Barenboim, M., Klein, S., Louzada, S., Banerjee, R., Strong, A., Stauber, T., Gross, N., Geumann, U., Lange, S., Ringelhan, M., Varela, I., Unger, K., Yang, F., Schmid, R.M., Vassiliou, G.S., Braren, R., Schneider, G., Heikenwalder, M., Bradley, A., Saur, D., Rad, R., 2016. Multiplexed pancreatic genome engineering and cancer induction by transfection-based CRISPR/Cas9 delivery in mice. Nat. Commun. 7, 10770. https://doi.org/10.1038/ncomms10770

Montironi, R., Lopez-Beltran, A., 2005. The 2004 WHO Classification of Bladder Tumors: A Summary and Commentary. Int. J. Surg. Pathol. 13, 143–153. https://doi.org/10.1177/106689690501300203

Mostofi, F.K., Sobin, L.H., Torloni, H., World Health Organization, 1973. Histological typing of urinary bladder tumours. World Health Organ., International histological classification of tumours ; no. 10.

Osei-Amponsa, V., Buckwalter, J.M., Shuman, L., Zheng, Z., Yamashita, H., Walter, V., Wildermuth, T., Ellis-Mohl, J., Liu, C., Warrick, J.I., Shantz, L.M., Feehan, R.P., Al-Ahmadie, H., Mendelsohn, C., Raman, J.D., Kaestner, K.H., Wu, X.-R., DeGraff, D.J., 2019. Hypermethylation of FOXA1 and allelic loss of PTEN drive squamous differentiation and promote heterogeneity in bladder cancer. Oncogene. https://doi.org/10.1038/s41388-019-1063-4

Papafotiou, G., Paraskevopoulou, V., Vasilaki, E., Kanaki, Z., Paschalidis, N., Klinakis, A., 2016. KRT14 marks a subpopulation of bladder basal cells with pivotal role in regeneration and tumorigenesis. Nat. Commun. 7, 11914. https://doi.org/10.1038/ncomms11914

Pietzak, E.J., Bagrodia, A., Cha, E.K., Drill, E.N., Iyer, G., Isharwal, S., Ostrovnaya, I., Baez, P., Li, Q., Berger, M.F., Zehir, A., Schultz, N., Rosenberg, J.E., Bajorin, D.F., Dalbagni, G., Al-Ahmadie, H., Solit, D.B., Bochner, B.H., 2017. Next-generation Sequencing of Nonmuscle Invasive Bladder Cancer Reveals Potential Biomarkers and Rational Therapeutic Targets. Eur. Urol. 72, 952–959. https://doi.org/10.1016/j.eururo.2017.05.032

Platt, F.M., Hurst, C.D., Taylor, C.F., Gregory, W.M., Harnden, P., Knowles, M.A., 2009. Spectrum of Phosphatidylinositol 3-Kinase Pathway Gene Alterations in Bladder Cancer. Clin. Cancer Res. 15, 6008–6017. https://doi.org/10.1158/1078-0432.CCR-09-0898

Platt, R.J., Chen, S., Zhou, Y., Yim, M.J., Swiech, L., Kempton, H.R., Dahlman, J.E., Parnas, O., Eisenhaure, T.M., Jovanovic, M., Graham, D.B., Jhunjhunwala, S., Heidenreich, M., Xavier, R.J., Langer, R., Anderson, D.G., Hacohen, N., Regev, A., Feng, G., Sharp, P.A., Zhang, F., 2014. CRISPR-Cas9 Knockin Mice for Genome Editing and Cancer Modeling. Cell 159, 440–455. https://doi.org/10.1016/j.cell.2014.09.014

Puzio-Kuter, A.M., Castillo-Martin, M., Kinkade, C.W., Wang, X., Shen, T.H., Matos, T., Shen, M.M., Cordon-Cardo, C., Abate-Shen, C., 2009. Inactivation of p53 and Pten promotes invasive bladder cancer. Genes Dev. 23, 675–680. https://doi.org/10.1101/gad.1772909

Qi, L.S., Larson, M.H., Gilbert, L.A., Doudna, J.A., Weissman, J.S., Arkin, A.P., Lim, W.A., 2013. Repurposing CRISPR as an RNA-Guided Platform for Sequence-Specific Control of Gene Expression. Cell 152, 1173–1183. https://doi.org/10.1016/j.cell.2013.02.022

Rebouissou, S., Bernard-Pierrot, I., de Reynies, A., Lepage, M.-L., Krucker, C., Chapeaublanc, E., Herault, A., Kamoun, A., Caillault, A., Letouze, E., Elarouci, N., Neuzillet, Y., Denoux, Y., Molinie, V., Vordos, D., Laplanche, A., Maille, P., Soyeux, P., Ofualuka, K., Reyal, F., Biton, A., Sibony, M., Paoletti, X., Southgate, J., Benhamou, S., Lebret, T., Allory, Y., Radvanyi, F., 2014. EGFR as a potential therapeutic target for a subset of muscle-invasive bladder cancers presenting a basal-like phenotype. Sci. Transl. Med. 6, 244ra91-244ra91. https://doi.org/10.1126/scitranslmed.3008970

Robertson, A.G., Kim, J., Al-Ahmadie, H., Bellmunt, J., Guo, G., Cherniack, A.D., Hinoue, T., Laird, P.W., Hoadley, K.A., Akbani, R., Castro, M.A.A., Gibb, E.A., Kanchi, R.S., Gordenin, D.A., Shukla, S.A., Sanchez-Vega, F., Hansel, D.E., Czerniak, B.A., Reuter, V.E., Su, X., de Sa Carvalho, B., Chagas, V.S., Mungall, K.L., Sadeghi, S., Pedamallu, C.S., Lu, Y., Klimczak, L.J., Zhang, J., Choo, C., Ojesina, A.I., Bullman, S., Leraas, K.M., Lichtenberg, T.M., Wu, C.J., Schultz, Nicholaus, Getz, G., Meyerson, M., Mills, G.B., McConkey, D.J., Weinstein, J.N.,

Kwiatkowski, D.J., Lerner, S.P., Akbani, R., Al-Ahmadie, H., Albert, M., Alexopoulou, I., Ally, A., Antic, T., Aron, M., Balasundaram, M., Bartlett, J., Baylin, S.B., Beaver, A., Bellmunt, J., Birol, I., Boice, L., Bootwalla, M.S., Bowen, J., Bowlby, R., Brooks, D., Broom, B.M., Bshara, W., Bullman, S., Burks, E., Cárcano, F.M., Carlsen, R., Carvalho, B.S., Carvalho, A.L., Castle, E.P., Castro, M.A.A., Castro, P., Catto, J.W., Chagas, V.S., Cherniack, A.D., Chesla, D.W., Choo, C., Chuah, E., Chudamani, S., Cortessis, V.K., Cottingham, S.L., Crain, D., Curley, E., Czerniak, B.A., Daneshmand, S., Demchok, J.A., Dhalla, N., Djaladat, H., Eckman, J., Egea, S.C., Engel, J., Felau, I., Ferguson, M.L., Gardner, J., Gastier-Foster, J.M., Gerken, M., Getz, G., Gibb, E.A., Gomez-Fernandez, C.R., Gordenin, D.A., Guo, G., Hansel, D.E., Harr, J., Hartmann, A., Herbert, L.M., Hinoue, T., Ho, T.H., Hoadley, K.A., Holt, R.A., Hutter, C.M., Jones, S.J.M., Jorda, M., Kahnoski, R.J., Kanchi, R.S., Kasaian, K., Kim, J., Klimczak, L.J., Kwiatkowski, D.J., Lai, P.H., Laird, P.W., Lane, B.R., Leraas, K.M., Lerner, S.P., Lichtenberg, T.M., Liu, J., Lolla, L., Lotan, Y., Lu, Y., Lucchesi, F.R., Ma, Y., Machado, R.D., Maglinte, D.T., Mallery, D., Marra, M.A., Martin, S.E., Mayo, M., McConkey, D.J., Meraney, A., Meyerson, M., Mills, G.B., Moinzadeh, A., Moore, R.A., Mora Pinero, E.M., Morris, S., Morrison, C., Mungall, K.L., Mungall, A.J., Myers, J.B., Naresh, R., O'Donnell, P.H., Ojesina, A.I., Parekh, D.J., Parfitt, J., Paulauskis, J.D., Sekhar Pedamallu, C., Penny, R.J., Pihl, T., Porten, S., Quintero-Aguilo, M.E., Ramirez, N.C., Rathmell, W.K., Reuter, V.E., Rieger-Christ, K., Robertson, A.G., Sadeghi, S., Saller, C., Salner, A., Sanchez-Vega, F., Sandusky, G., Scapulatempo-Neto, C., Schein, J.E., Schuckman, A.K., Schultz, Nikolaus, Shelton, C., Shelton, T., Shukla, S.A., Simko, J., Singh, P., Sipahimalani, P., Smith, N.D., Sofia, H.J., Sorcini, A., Stanton, M.L., Steinberg, G.D., Stoehr, R., Su, X., Sullivan, T., Sun, Q., Tam, A., Tarnuzzer, R., Tarvin, K., Taubert, H., Thiessen, N., Thorne, L., Tse, K., Tucker, K., Van Den Berg, D.J., van Kessel, K.E., Wach, S., Wan, Y., Wang, Z., Weinstein, J.N., Weisenberger, D.J., Wise, L., Wong, T., Wu, Y., Wu, C.J., Yang, L., Zach, L.A., Zenklusen, J.C., Zhang, J. (Julia), Zhang, J., Zmuda, E., Zwarthoff, E.C., 2017. Comprehensive Molecular Characterization of Muscle-Invasive Bladder Cancer. Cell 171, 540-556.e25. https://doi.org/10.1016/j.cell.2017.09.007

Saito, R., Smith, C.C., Utsumi, T., Bixby, L.M., Kardos, J., Wobker, S.E., Stewart, K.G., Chai, S., Manocha, U., Byrd, K.M., Damrauer, J.S., Williams, S.E., Vincent, B.G., Kim, W.Y., 2018. Molecular Subtype-Specific Immunocompetent Models of High-Grade Urothelial Carcinoma Reveal Differential Neoantigen Expression and Response to

Immunotherapy. Cancer Res. 78, 3954–3968. https://doi.org/10.1158/0008-5472.CAN-18-0173

Saito, T., Nakatsuji, N., 2001. Efficient Gene Transfer into the Embryonic Mouse Brain Using in Vivo Electroporation. Dev. Biol. 240, 237–246. https://doi.org/10.1006/dbio.2001.0439

Sanli, O., Dobruch, J., Knowles, M.A., Burger, M., Alemozaffar, M., Nielsen, M.E., Lotan, Y., 2017. Bladder cancer. Nat. Rev. Dis. Primer 3, 17022. https://doi.org/10.1038/nrdp.2017.22

Scholzen, T., Gerdes, J., 2000. The Ki-67 protein: from the known and the unknown. J. Cell. Physiol. 182, 311–322. https://doi.org/10.1002/(SICI)1097-4652(200003)182:3<311::AID-JCP1>3.0.CO;2-9

Seiler, R., Ashab, H.A.D., Erho, N., van Rhijn, B.W.G., Winters, B., Douglas, J., Van Kessel, K.E., Fransen van de Putte, E.E., Sommerlad, M., Wang, N.Q., Choeurng, V., Gibb, E.A., Palmer-Aronsten, B., Lam, L.L., Buerki, C., Davicioni, E., Sjödahl, G., Kardos, J., Hoadley, K.A., Lerner, S.P., McConkey, D.J., Choi, W., Kim, W.Y., Kiss, B., Thalmann, G.N., Todenhöfer, T., Crabb, S.J., North, S., Zwarthoff, E.C., Boormans, J.L., Wright, J., Dall'Era, M., van der Heijden, M.S., Black, P.C., 2017. Impact of Molecular Subtypes in Muscle-invasive Bladder Cancer on Predicting Response and Survival after Neoadjuvant Chemotherapy. Eur. Urol. 72, 544–554. https://doi.org/10.1016/j.eururo.2017.03.030

Shin, K., Lee, J., Guo, N., Kim, J., Lim, A., Qu, L., Mysorekar, I.U., Beachy, P.A., 2011. Hedgehog/Wnt feedback supports regenerative proliferation of epithelial stem cells in bladder. Nature 472, 110–114. https://doi.org/10.1038/nature09851

Shorning, B.Y., Griffiths, D., Clarke, A.R., 2011. Lkb1 and Pten Synergise to Suppress mTOR-Mediated Tumorigenesis and Epithelial-Mesenchymal Transition in the Mouse Bladder. PLoS ONE 6, e16209. https://doi.org/10.1371/journal.pone.0016209

Siegel, R.L., Miller, K.D., Jemal, A., 2019. Cancer statistics, 2019. CA. Cancer J. Clin. 69, 7–34. https://doi.org/10.3322/caac.21551

Sjödahl, G., Eriksson, P., Liedberg, F., Höglund, M., 2017. Molecular classification of urothelial carcinoma: global mRNA classification versus tumour-cell phenotype classification: Urothelial carcinoma classification. J. Pathol. 242, 113–125. https://doi.org/10.1002/path.4886

Solomon, D.A., Kim, J.-S., Bondaruk, J., Shariat, S.F., Wang, Z.-F., Elkahloun, A.G., Ozawa, T., Gerard, J., Zhuang, D., Zhang, S., Navai, N., Siefker-Radtke, A., Phillips, J.J., Robinson, B.D., Rubin, M.A., Volkmer, B., Hautmann, R., Küfer, R., Hogendoorn, P.C.W., Netto, G., Theodorescu, D., James, C.D., Czerniak, B., Miettinen, M., Waldman, T., 2013. Frequent truncating mutations of STAG2 in bladder cancer. Nat. Genet. 45, 1428–1430. https://doi.org/10.1038/ng.2800

Spruck, C.H., Ohneseit, P.F., Gonzalez-Zulueta, M., Esrig, D., Miyao, N., Tsai, Y.C., Lerner, S.P., Schmütte, C., Yang, A.S., Cote, R., 1994. Two molecular pathways to transitional cell carcinoma of the bladder. Cancer Res. 54, 784–788.

Stewart, F.A., Denekamp, J., Hirst, D.G., 1980. PROLIFERATION KINETICS OF THE MOUSE BLADDER AFTER IRRADIATION. Cell Prolif. 13, 75–89. https://doi.org/10.1111/j.1365-2184.1980.tb00451.x

Sun, W., Wilhelmina Aalders, T., Oosterwijk, E., 2014. Identification of potential bladder progenitor cells in the trigone. Dev. Biol. 393, 84–92. https://doi.org/10.1016/j.ydbio.2014.06.018

Taylor, C.F., Platt, F.M., Hurst, C.D., Thygesen, H.H., Knowles, M.A., 2014. Frequent inactivating mutations of STAG2 in bladder cancer are associated with low tumour grade and stage and inversely related to chromosomal copy number changes. Hum. Mol. Genet. 23, 1964–1974. https://doi.org/10.1093/hmg/ddt589

Tomlinson, D., Baldo, O., Harnden, P., Knowles, M., 2007. FGFR3 protein expression and its relationship to mutation status and prognostic variables in bladder cancer. J. Pathol. 213, 91–98. https://doi.org/10.1002/path.2207

van Oers, J.M.M., Adam, C., Denzinger, S., Stoehr, R., Bertz, S., Zaak, D., Stief, C., Hofstaedter, F., Zwarthoff, E.C., van der Kwast, T.H., Knuechel, R., Hartmann, A., 2006. Chromosome 9 deletions are more frequent

thanFGFR3 mutations in flat urothelial hyperplasias of the bladder. Int. J. Cancer 119, 1212–1215. https://doi.org/10.1002/ijc.21958

Veranič, P., Erman, A., Kerec-Kos, M., Bogataj, M., Mrhar, A., Jezernik, K., 2009. Rapid differentiation of superficial urothelial cells after chitosan-induced desquamation. Histochem. Cell Biol. 131, 129–139. https://doi.org/10.1007/s00418-008-0492-x

Wang, H., La Russa, M., Qi, L.S., 2016. CRISPR/Cas9 in Genome Editing and Beyond. Annu. Rev. Biochem. 85, 227–264. https://doi.org/10.1146/annurev-biochem-060815-014607

Weber, J., Öllinger, R., Friedrich, M., Ehmer, U., Barenboim, M., Steiger, K., Heid, I., Mueller, S., Maresch, R., Engleitner, T., Gross, N., Geumann, U., Fu, B., Segler, A., Yuan, D., Lange, S., Strong, A., de la Rosa, J., Esposito, I., Liu, P., Cadiñanos, J., Vassiliou, G.S., Schmid, R.M., Schneider, G., Unger, K., Yang, F., Braren, R., Heikenwälder, M., Varela, I., Saur, D., Bradley, A., Rad, R., 2015. CRISPR/Cas9 somatic multiplex-mutagenesis for high-throughput functional cancer genomics in mice. Proc. Natl. Acad. Sci. 112, 13982–13987. https://doi.org/10.1073/pnas.1512392112

Wu, X.-R., Kong, X.-P., Pellicer, A., Kreibich, G., Sun, T.-T., 2009. Uroplakins in urothelial biology, function, and disease. Kidney Int. 75, 1153–1165. https://doi.org/10.1038/ki.2009.73

Xue, W., Chen, S., Yin, H., Tammela, T., Papagiannakopoulos, T., Joshi, N.S., Cai, W., Yang, G., Bronson, R., Crowley, D.G., Zhang, F., Anderson, D.G., Sharp, P.A., Jacks, T., 2014. CRISPR-mediated direct mutation of cancer genes in the mouse liver. Nature 514, 380–384. https://doi.org/10.1038/nature13589

Yang, Z., Li, C., Fan, Z., Liu, H., Zhang, X., Cai, Z., Xu, L., Luo, J., Huang, Y., He, L., Liu, C., Wu, S., 2017. Single-cell Sequencing Reveals Variants in ARID1A, GPRC5A and MLL2 Driving Self-renewal of Human Bladder Cancer Stem Cells. Eur. Urol. 71, 8–12. https://doi.org/10.1016/j.eururo.2016.06.025

Yeung, C., Dinh, T., Lee, J., 2014. The Health Economics of Bladder Cancer: An Updated Review of the Published Literature. PharmacoEconomics 32, 1093–1104. https://doi.org/10.1007/s40273-014-0194-2

Yu, C., Stefanson, O., Liu, Y., Wang, Z.A., 2018. Novel Method of Plasmid DNA Delivery to Mouse Bladder Urothelium by Electroporation. J. Vis. Exp. https://doi.org/10.3791/57649

Zhao, C., 2006. Distinct Morphological Stages of Dentate Granule Neuron Maturation in the Adult Mouse Hippocampus. J. Neurosci. 26, 3–11. https://doi.org/10.1523/JNEUROSCI.3648-05.2006

Zuckermann, M., Hovestadt, V., Knobbe-Thomsen, C.B., Zapatka, M., Northcott, P.A., Schramm, K., Belic, J., Jones, D.T.W., Tschida, B., Moriarity, B., Largaespada, D., Roussel, M.F., Korshunov, A., Reifenberger, G., Pfister, S.M., Lichter, P., Kawauchi, D., Gronych, J., 2015. Somatic CRISPR/Cas9-mediated tumour suppressor disruption enables versatile brain tumour modelling. Nat. Commun. 6, 7391. https://doi.org/10.1038/ncomms8391